PROFILING AND RESCUE OF DISEASE-RELEVANT ELECTROPHYSIOLOGICAL AND MORPHOLOGICAL PHENOTYPES IN NEURONS OF TRANSGENIC MOUSE MODELS OF SCHIZOPHRENIA

Michaela Inanna Warnhoff

Graduate School of
Systemic Neurosciences

LMU Munich

Dissertation at the
Graduate School of Systemic Neurosciences
Ludwig-Maximilians-Universität München

17.07.2023

Profiling and rescue of disease-relevant electrophysiological and morphological phenotypes in neurons of transgenic mouse models of schizophrenia

Michaela Inanna Warnhoff

Dissertation at the
Graduate School of Systemic Neurosciences
Ludwig-Maximilians-Universität München

17.07.2023

Supervisor
PD Dr. Volker Scheuss
Department of Molecular Neurobiology
LMU Clinic for Psychiatry and Psychotherapy
Nussbaumstraße 7
80336 Munich

First Reviewer: PD Dr. Volker Scheuss
Second Reviewer: Prof. Dr. Laura Busse
External Reviewer: Prof. Dr. Veronica Egger
Date of Submission: 17.07.2023
Date of Defense: 20.02.2024

Abstract

Schizophrenia is a debilitating mental disorder caused by a combination of genetic and environmental factors. It is characterized by a triad of positive, negative, and cognitive symptoms: These can include delusions and hallucinations, social withdrawal and anhedonia, and broad attentional, executive, language, and memory impairments, respectively. The molecular and cellular correlates of these cognitive impairments and changes in neuronal circuit connectivity associated with them include altered neurotransmission in the prefrontal cortex, impaired synaptic plasticity, and aberrant neuronal morphology, contributing to functional and structural dysconnectivity between brain regions. However, they are still poorly understood. Treatment approaches mainly focus on alleviating positive symptoms. Cognitive symptoms, however, are largely resistant to current treatment and often persist or worsen throughout life. Thus, they constitute a major determinant of the extent of functional disability and long-term prognosis.

To study cellular correlates of cognitive symptoms and novel treatment approaches and their specific mode of action, I used transgenic mouse models of schizophrenia focusing on the mPFC, a hub for higher cognitive functions. One of these models is the *Neurod6* KO mouse. NEUROD6 is a transcription factor involved in neuronal differentiation and development of the nervous system predominantly expressed in excitatory neurons. It interacts with the well-known *TCF4* risk gene for schizophrenia and is downregulated in DLPFC pyramidal neurons in schizophrenic patients. *Neurod6* KO mice display increased behavioral impulsivity and hyperactivity. Here, I focused on electrophysiological correlates of these behavioral phenotypes, the pharmacological rescue of electrophysiological phenotypes paralleling the pharmacological rescue of behavioral phenotypes, and the mode of action of effective pharmacological compounds. Performing whole-cell patch-clamp recordings in acute brain slices in L5 output neurons in the PL of the mPFC, I found neuronal hyperexcitability and a disturbed use-dependent action potential generation. The latter was rescued by application of the tricyclic antidepressant protriptyline and DPO-1, a specific Kv1.5-blocker. This hints at a possible depolarization block in *Neurod6* KO neurons which may contribute to the observed behavioral phenotypes.

Additionally, I used another mouse model – the *Taok2*xEmx1-Cre conditional KO mouse. TAOK2 is a serine/threonine protein kinase involved in microtubule stability, and mutations on the *TAOK2* gene carry susceptibility to schizophrenia and autism spectrum disorders. Moreover, TAOK2 downregulation has been shown to affect spine density and dendrite formation, structures important for neuron-neuron communication and circuit integration. Thus, I focused on the influence of cre-dependent KO of *Taok2* on morphological characteristics and circuit integration of neurons. To this end, I performed

whole-cell patch-clamp recordings and 2-Photon imaging in acute brain slices in L5 output neurons in the PL of the mPFC and primary neuronal cortical cultures from *Taok2*xEmx1-Cre KO mice. Interestingly, there was no effect of Cre-conditional KO of *Taok2* on the complexity of dendritic arborization, spine density, or synaptic integration in acute slices. However, the complexity of dendritic arborization was reduced in primary neuronal cortical cultures. Compensatory mechanisms might be at play in the live organism, or other layers than those investigated might be affected.

In summary, these findings may contribute to the understanding of cognitive symptoms in schizophrenia and novel approaches regarding their treatment.

Keywords: schizophrenia, cognitive impairment, impulsivity, medial prefrontal cortex, prelimbic cortex, NEUROD6, TAOK2, hyperexcitability, sustained action potential firing, depolarization block, protriptyline, DPO-1, Kv1.5, dendritic arborization, spine density, circuit integration, whole-cell patch-clamp recordings, 2-photon imaging

Table of contents

List of figures

List of tables

Abbreviations

In the order of the first appearance:

mPFC	Medial prefrontal cortex
***NEUROD*/*Neurod*/NEUROD**	Neuronal differentiation factor
KO	Knock-out
***TCF4*/TCF4**	Transcription factor 4
DLPFC	Dorsolateral prefrontal cortex
L	Cortical layer
PL	Prelimbic cortex
DPO-1	Diphenyl phosphine oxide-1
Kv1.5	Voltage-gated potassium channel 1.5
***TAOK*/*Taok*/TAOK**	Thousand and one amino acid protein kinase
ctrl	Control
VLPFC	Ventrolateral prefrontal cortex
OFC	Orbitofrontal cortex
NMDAR	N-methyl-D-aspartate receptor
ACC	Anterior cingulate cortex
IL	Infralimbic cortex
ADHD	Attention deficit hyperactivity disorder
PsyCoP	Platform for systematic cognitive and behavioral profiling
bHLH	Basic helix-loop-helix
neoR	Neomycin resistance gene
FDA	Food and drug administration
MAP3K	Mitogen-activated protein kinase kinase kinase
DIV	Day-in-vitro
P	Postnatal day
TTX	Tetrodotoxin
AAV	Adeno-associated virus

mEPSCs	Miniature excitatory postsynaptic currents
mIPSCs	Miniature inhibitory postsynaptic currents
Vm rest	Resting membrane potential
SD	Standard deviation
s.e.m.	Standard error of the mean
snRNAseq	Single nucleus RNA sequencing
a-AP	4-aminopyridine
TEA	Tetraethylammonium
CA1	Hippocampal cornu ammonis 1
STN	Subthalamic nucleus
LH	Lateral hypothalamus
VTA	Ventral tegmental area
ERK	Extracellular-signal regulated kinase
JNK	c-Jun-N-terminal kinase
GABA	γ-aminobutanoic acid

1 Introduction

1.1 Schizophrenia

1.1.1 Schizophrenia: A life-long burden

Schizophrenia is a complex mental disorder caused by a combination of genetic and environmental factors. Even though its global age-standardized point prevalence is low – estimated to be 0.28 % in 2016 – its disease burden is substantial: It contributes 13.4 million years of life lived with a disability to the burden of disease globally (Charlson et al., 2018). Additionally, treatment outcomes are poor: A systematic review based on 50 studies found the median proportion of people with schizophrenia meeting recovery criteria to be only 13.5 % (Jaaskelainen et al., 2013). Furthermore, the majority of affected individuals experience schizophrenia as a chronic recurrent disease with increasing residual morbidity in-between psychotic episodes, and with behavioral deterioration (Lieberman et al., 1996).

1.1.2 Positive, negative, and cognitive symptoms

Schizophrenia is characterized by a triad of positive, negative, and cognitive symptoms. Positive symptoms can include delusions and hallucinations, i.e., abnormalities regarding perception and the interpretation of reality. Negative symptoms include affective flattening, social withdrawal, and anhedonia, and cognitive symptoms comprise a cluster of broad attentional, executive, language, and memory impairments. Among the most impaired cognitive domains are attention and executive functions (Cirillo & Seidman, 2003). Several studies emphasize increased impulsivity in patients with schizophrenia, be it assessed by self-report questionnaires or behavioral paradigms (e.g., Ouzir, 2013, for a review). For example, schizophrenic patients score higher than healthy subjects on the Barratt Impulsivity Scale (BIS) (Enticott, Ogloff, & Bradshaw, 2008; Kaladjian, Jeanningros, Azorin, Anton, & Mazzola-Pomietto, 2011), and they present significant deficits in the ability to inhibit premature responses in go/no-go and stop-signal tasks (Lipszyc & Schachar, 2010; Nolan, D'Angelo, & Hoptman, 2011) or regarding choice impulsivity or delay discounting (Heerey, Robinson, McMahon, & Gold, 2007). Other studies emphasize impairments in the triggering of inhibitory processes (Badcock, Michie, Johnson, & Combrinck, 2002).

Even though the positive symptoms are the most dramatic and recognizable symptoms of schizophrenia, it is the cognitive impairments that most affect an individual's ability to function efficiently in daily life. Almost 98 % of schizophrenia patients (Keefe, Eesley, & Poe, 2005) have such impairments, and they present early in the disease – even before clinical diagnosis (Sakurai et al., 2015).

Cognitive impairments constitute a major determinant of the extent of disability and long-term prognosis (Simpson, Kellendonk, & Kandel, 2010). Impulsivity, in particular, increases hospitalization, treatment challenge, physical harm (Jung et al., 2022), and maladaptive behavior like substance abuse, exacerbating psychotic symptoms and resulting in more frequent suicide attempts (Gut-Fayand et al., 2001).

1.1.3 The prefrontal cortex and cognitive symptoms in schizophrenia

The prefrontal cortex is involved in a variety of higher cognitive functions. Among these are executive functions like attention, behavioral inhibition, and impulsivity. A study by Blasi et al. (2006), for example, found activation in DLPFC, VLPFC, and other frontal areas during response inhibition. The prefrontal cortex is also involved in learning and memory, e.g., working memory, and categorization (Euston, Gruber, & McNaughton, 2012). Prefrontal cortex dysfunction has long been implicated in cognitive deficits in schizophrenia patients. Among the first indications of this is a study by Kolb and Whishaw (1983), reporting that findings in patients with schizophrenia parallel findings in patients with frontal lobe damage. Furthermore, there has been a variety of studies suggesting that cognitive dysfunction is attributable to prefrontal cortex metabolic hypofunction (e.g., Farkas et al., 1984; Ingvar & Franzen, 1974; Ragland, Yoon, Minzenberg, & Carter, 2007). Regarding impulsivity specifically, Leclerc, Regenbogen, Hamilton, and Habel (2018) emphasize deficits associated with impaired decision making especially in VLPFC and OFC in patients with aggressive schizophrenia. Poor executive control in schizophrenia has also been related to hypoactivity of the thalamus co-occurring with DLPFC hypoactivation (Minzenberg, Laird, Thelen, Carter, & Glahn, 2009).

Schizophrenia in general is thought to arise from disrupted brain connectivity and abnormal interactions within and between prefrontal cortical and subcortical structures rather than from regionally-specific pathophysiology (Andreasen, Paradiso, & O'Leary, 1998; Friston, 1998; Pettersson-Yeo, Allen, Benetti, McGuire, & Mechelli, 2011). In line with this, Callicott et al. (2003) showed that, in an N-back working memory test, several areas within the prefrontal cortex in low-performing patients were less active than in control subjects. Thus, low-performing patients potentially failed to sustain activation in the prefrontal processing network. Within the prefrontal cortex of high-performing patients, however, there were hypo- and hyperactive areas, reflecting a need for engaging greater prefrontal resources as a compensatory mechanism. Similarly, Ragland, Yoon, Minzenberg, and Carter (2007) suggested that hypoactivation of the DLPFC and hyperactivation of adjacent regions might go hand-in-hand, confirming a disturbed ability to engage executive functional networks. Disrupted functional connectivity between DLPFC and parietal regions may explain impaired executive function

and cognitive control in schizophrenia (Zhou, Fan, Qiu, & Jiang, 2015). Andreasen, Paradiso, and O'Leary (1998) implicate a more general processing network comprised of prefrontal regions, the thalamic nuclei, and the cerebellum, hypothesizing that dysfunction within this circuitry results in difficulty in prioritizing, processing, coordinating, and responding to information. According to the authors, this difficulty accounts for the broad range of cognitive symptoms in schizophrenia.

1.1.4 Molecular, cellular, and neuronal network correlates of cognitive symptoms in schizophrenia

The molecular and cellular correlates of cognitive impairments and changes in neuronal circuit connectivity associated with them have been investigated; however, they are still poorly understood.

Several studies in non-human primates (see, e.g., Brozoski, Brown, Rosvold, & Goldman, 1979; Vijayraghavan, Wang, Birnbaum, Williams, & Arnsten, 2007) and in humans (Abi-Dargham et al., 2002; Barnett, Jones, Robbins, & Muller, 2007; Weinberger, Berman, & Illowsky, 1988) exist pointing towards dopamine hypoactivity in the prefrontal cortex in schizophrenia. However, these studies mostly comprise indirect observations, and direct dopamine release in the prefrontal cortex has not been measured so far. Further, there is no direct evidence derived from studies with patients.

The serotonergic system has been implicated in working memory, attention, decision-making, and reversal learning as well (Clark, Cools, & Robbins, 2004; Robbins, 2000), albeit in a more indirect manner: It has been reported that serotonergic pathways ascending towards the prefrontal cortex are upregulated in schizophrenia, leading to the previously mentioned dopamine hypoactivity (for a review, see Kapur & Remington, 1996).

Moreover, a dysfunction or dysregulation of glutamate NMDAR-mediated neurotransmission due to receptor hypofunction has been suggested. This dysregulation impairs synaptic plasticity and affects dopaminergic and other systems (Kantrowitz & Javitt, 2010). In line with this, major findings regarding neuronal morphology in schizophrenia include spine loss and atrophied dendrites of prefrontal neurons, and reduced prefrontal grey matter in general (Zhou et al., 2015). Such aberrant morphology might contribute to the disrupted functional connectivity of brain regions.

However, not much is known about the electrophysiological functioning of prefrontal neurons related to disturbed executive behavior.

1.1.5 Current pharmacological treatment approaches

Current pharmacological treatment of schizophrenia mainly focuses on alleviating positive symptoms. All established antipsychotic medications antagonize dopamine D2 receptors and are very effective in reducing the severity of hallucinations and delusions. However, cognitive impairment is largely resistant to such treatment: It persists or even worsens throughout life. This is not surprising,

given that dopamine receptor antagonism would contribute to dopamine hypofunction. There are currently no approved treatments for neurocognitive impairment in schizophrenia and related disorders (Keefe et al., 2007).

Furthermore, there is no consensus yet on optimal disease-relevant drug targets. Targets under investigation include those acting upon key brain receptors (e.g., serotonergic receptor antagonists) and those activating intracellular signaling cascades involved in memory (e.g., phosphodiesterase inhibitors) (Wallace, Ballard, Pouzet, Riedel, & Wettstein, 2011), or NMDAR modulators like D-serine or glycine (e.g., Singh & Singh, 2011). However, there are no drugs targeting specific executive functions, and no other drug targets have been explored.

1.2 Transgenic mouse models of schizophrenia

1.2.1 Limitations and possibilities of using mouse models to study schizophrenia

Many genes and molecular pathways involved in schizophrenia have been identified, and transgenic mouse models targeting these pathways can be used to relate molecular changes to cellular and circuit alterations and behavioral phenotypes. Furthermore, mouse models can be used for treatment screening approaches. It is important to note here that transgenic mouse models usually focus on one particular pathway or risk gene and never fully replicate human pathology arising from the combination of several pathway disturbances and alterations. However, this makes it possible to look at specific alterations and their downstream effects separately. Additionally, positive symptoms like hallucinations, delusions, and thought disturbances representing the loss of reality occurring when entering a state of psychosis are difficult to measure in the mouse. Thus, the focus lies on modeling negative and cognitive symptoms for which standardized behavioral tests are available.

1.2.2 The rodent mPFC as a hub for higher cognitive functions

In rodents, the mPCF consists of the ACC, the PL, and the IL (Fig. **1.1**). It can be subdivided into dorsal (ACC) and ventral (PL, IL) regions with distinct functions: The dorsal region is involved in memory for motor responses encompassing response selection and temporal information processing. The ventral region is involved in attentional processes, e.g., attention to stimulus features and task contingencies, set-shifting, and behavioral flexibility (Bissonette, Powell, & Roesch, 2013; Dalley, Cardinal, & Robbins, 2004; Heidbreder & Groenewegen, 2003; Vertes, 2006). Both PL and IL are involved in impulsive behavior: Studies mostly implicate the IL in impulsive action, waiting, and premature responses (Chudasama, 2011; Chudasama et al., 2003; Jupp et al., 2013; Robbins, 2002;

Sokolowski & Salamone, 1994). However, stopping an action that has been initiated and perseverative responses depend on PL (Feja & Koch, 2015; Turner & Parkes, 2020).

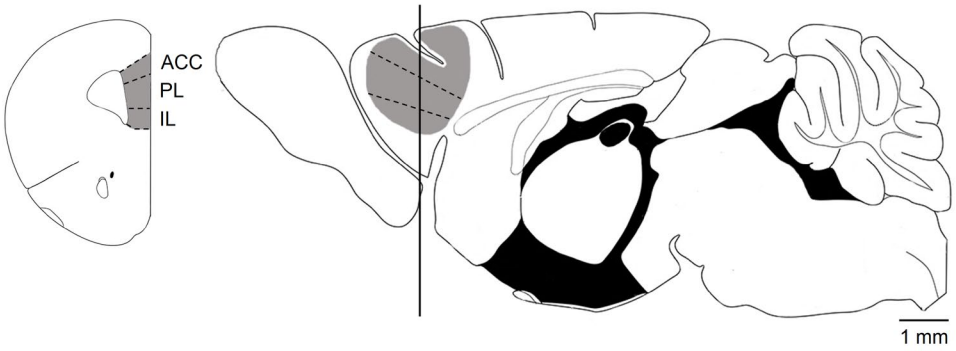

Figure 1.1 The rodent mPFC and its subdivisions.

Left, coronal section through the rodent brain. Schematic taken from Paxinos and Franklin (2001) and modified**,** + 1.98 mm from Bregma. Right, sagittal section through the rodent brain. Schematic taken from Paxinos and Franklin (2001) and modified. Black line, line of coronal cut at 1.98 mm from Bregma. Grey area, mPFC.

1.2.3 Neurod6 KO model

NEUROD6/Neurod6 is one of the most specific marker genes of cortical and hippocampal projection neurons in humans as well as in the mouse (Bormuth et al., 2013). NEUROD6 is a member of the functionally redundant NEUROD transcription factor family (Schwab et al., 1998). It is involved in neuronal differentiation and nervous system development. To become transcriptionally active, it needs to form heterodimers with other bHLH proteins, among them the TCF4 protein encoded by the well-known risk gene for schizophrenia *TCF4* (Kepa et al., 2017). NEUROD6 is downregulated by > 40 % in DLPFC L3 and L5 pyramidal neurons in post-mortem tissue from schizophrenic patients (Arion et al., 2015). Moreover, it has been associated with ADHD due to its role in brain lateralization (Bonvicini, Faraone, & Scassellati, 2018).

In *Neurod6* full KO mice, most of the *Neurod6* coding region (residues 53 - 337, including the bHLH domain) is replaced by neoR (Schwab et al., 1998). *Neurod6* KO mice were characterized behaviorally with PsyCoP (a test battery developed by Volkmann, Stephan, Krackow, Jensen, & Rossner, 2020) by colleagues at the clinic. These mice exhibited behavioral hyperactivity ($P = 1.8 \times 10^{-6}$, one-way ANOVA; Fig. **1.2.A**, top panel) and disturbed executive functioning as evidenced by increased impulsivity in a waiting task ($P = 1.4 \times 10^{-5}$ and $P = .009$, at delays of 0.5 and 1.5 s, respectively, one-way

ANOVAs; Fig. **1.2.A**, bottom panel). At the clinic, the FDA-approved compound paliperidone, an atypical antipsychotic, was found to selectively rescue behavioral hyperactivity (P = .023, Wilcoxon rank-sum test; Fig. **1.2.B**, top panel). Conversely, protriptyline, a tricyclic antidepressant, selectively rescued impulsivity (P = .008 and P = 9.1 x 10^{-4}, at delays of 0.5 and 1.5 s, respectively, Wilcoxon rank-sum tests; Fig. **1.2.B**, bottom panel). Thus, hypothesizing that the physiology of prefrontal neurons involved in cognitive functioning may be altered in *Neurod6* KO, these compounds, especially protriptyline, represent promising candidates for a validation on the cellular level.

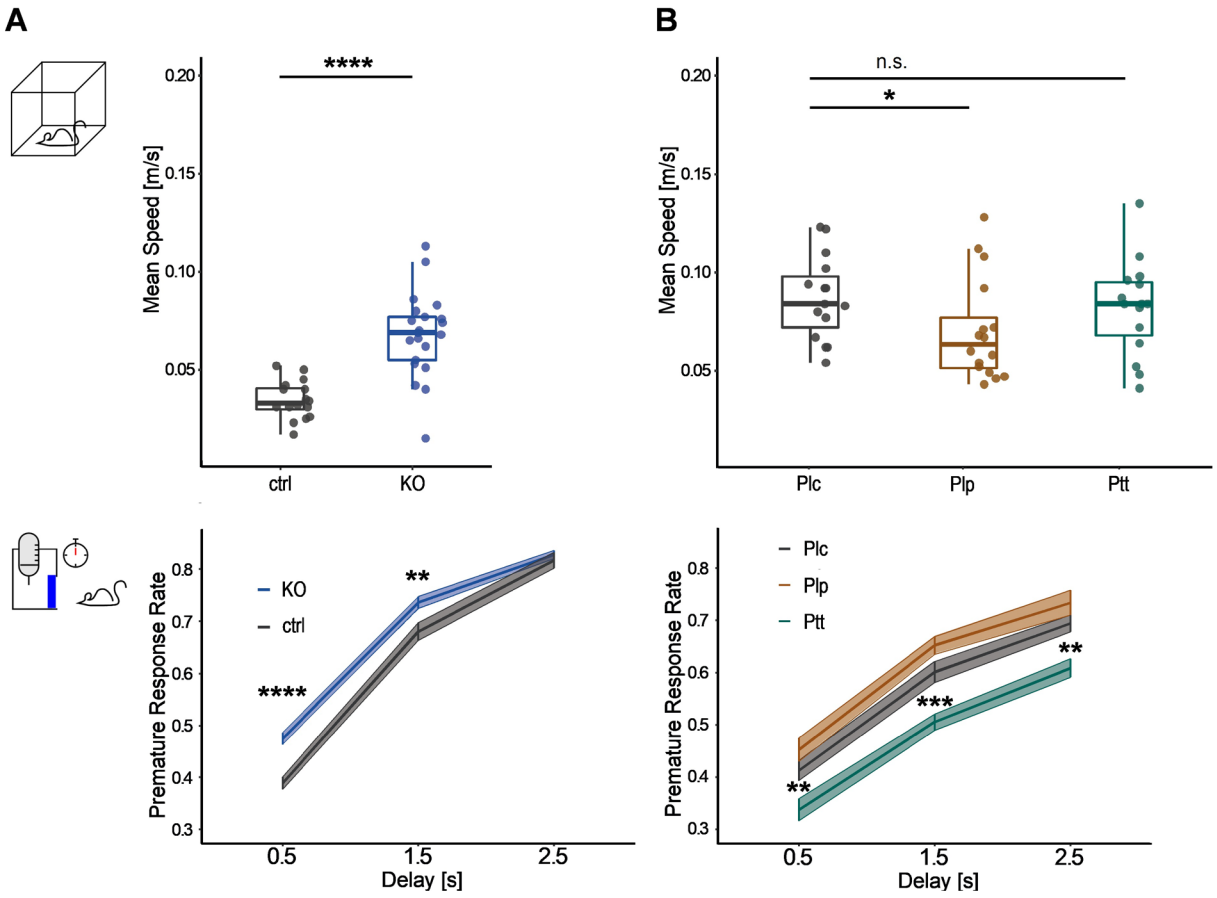

Figure 1.2 *Neurod6* KO mice show behavioral disturbances that can be rescued pharmacologically.

A. Top, *Neurod6* KO mice (n = 21) showed an increased mean speed in the open field compared to ctrl (n = 16), P = 1.8 x 10^{-6}. Thick horizontal lines, medians, boxes and whiskers, interquartile ranges. Inset, open field. Bottom, at a delay of 0.5 s and 1.5 s, *Neurod6* KO mice (n = 21) showed an increased rate of premature responses compared to ctrl (n = 16), P = 1.4 x 10^{-5} and P = .009, respectively. Vertical error bars, means ± s.e.m., colored areas, areas between means ± s.e.m. Inset, waiting task: Mice gained access to a water bottle behind a door (blue bar) after a waiting period (delay) after a nose poke. To enter, they had to give another nose poke. Premature

responses were defined as nose pokes before the end of the delay. **B.** Top, Plp selectively rescued mean speed. Mean speed was significantly decreased in Plp-treated KO (*n* = 16) compared to Plc-treated KO (*n* = 16), *P* = .023. In contrast, Ptt-treated KO (*n* = 16) had a similar mean speed as Plc-treated KO, *P* = .51. Thick horizontal lines, medians, boxes and whiskers, interquartile ranges. Bottom, Ptt selectively rescued the rate of premature responses. At a delay of 0.5 s, 1.5 s, and 2.5 s, Ptt-treated KO (*n* = 16) displayed a significantly lower rate of premature responses than Plc-treated KO (*n* = 16), *P* = .008, *P* = 9.1 x 10^{-4}, and *P* = .003, respectively. The rate of premature responses between Plp-treated KO (*n* = 16) and Plc-treated KO (*n* = 16) was similar at all three delays, *P* = .13, *P* = .094, and *P* = .24, respectively. Vertical error bars, means ± s.e.m., colored areas, areas between means ± s.e.m. Note: Data for **1.2.A** and **1.2.B** were obtained from different cohorts of mice. Differences in baseline behavior between cohorts can result from uncontrollable variability in birthing, rearing, or housing conditions, e.g. birth complications, number of littermates, or number of co-housed mice.

Plc, placebo, *Plp*, paliperidone, *Ptt*, protriptyline, *, *P* < .05, **, *P* < .01, ***, *P* < .001, ****, *P* < .0001, n.s., not significant. One-way ANOVAs and Wilcoxon rank-sum tests. Filled circles, individual mouse data. All data were acquired by colleagues at the clinic (Philipp Schuler and Marius Stephan). All plots are used with permission from Marius Stephan.

1.2.4 Taok2 x Emx1-Cre KO model

TAOKs (serine/threonine-protein kinases) are members of the MAP3K family. In mammals, TAOK1, 2, and 3 have been identified. All of them are involved in similar pathways, and especially TAOK1 and 2 have been involved in the regulation of cytoskeleton components and microtubule stability, processes important for early brain development (Fang, Lai, Hsiao, & Chang, 2020). Here, I will focus on TAOK2 and its two isoforms, TAOK2α and TAOK2β (de Anda et al., 2012; Scharrenberg et al., 2022; Yasuda et al., 2007).

TAOK2 is a candidate risk gene for neurodevelopmental disorders: The *TAOK2* gene is located on the chromosome 16p11.2 locus carrying susceptibility to schizophrenia and autism spectrum disorders (McCarthy et al., 2009). In line with the hypothesis of atypical brain connectivity and deficits regarding synaptic plasticity and transmission in schizophrenia, TAOK2 has been implicated in processes regulating spine and synapse development, maintenance, and maturation, and in basal dendrite formation. Ultanir et al. (2014), for example, showed an increase in filopodia number and length, and a reduction of spines following TAOK2 downregulation once spine formation had already taken place. The authors also demonstrated the importance of TAOK2 for limiting filopodia formation during development. These studies were done in hippocampal neuronal cultures; however, they found TAOK2 to also be important for spine formation on L2/3 cortical neurons *in vivo*: Spine density in the adolescent mouse was decreased upon downregulation of TAOK2 *in utero*.

De Anda et al. (2012) demonstrated a decreased number of primary and secondary neurites in primary cortical neurons at DIV2 following TAOK2α downregulation *in utero*. Similarly, they showed fewer primary basal dendrites and less complex basal dendritic arborization in cortical neurons from P7 mice after *in utero* electroporation. There were no effects on apical dendrites. In experiments done in neuronal culture, TAOK2β has also been implicated in a homeostatic mechanism that balances the complexity of neuronal networks by regulating the adhesiveness of synaptic membranes, eliminating superfluous spines during a recovery phase after stimulation (Yasuda et al., 2007).

Finally, using heterozygous and full *Taok2* KO mice, Richter et al. (2019) found effects of TAOK2 downregulation on brain size in cortical regions and on neural connectivity in the PFC and hippocampus, as well as on memory-related cognition and cognitive flexibility: In a gene dosage-dependent manner, brain size and connectivity were reduced, and cognition was impaired. These mice also have deficits in basal dendritic complexity, and they show reduced basal spine density and reduced excitatory neurotransmission in L2 neurons of the ACC and the PL of the PFC.

The *Taok2* (floxed/floxed) x Emx1-Cre KO strain was newly generated at the clinic by Michael Wehr. In these mice, *Taok2* is knocked out once Cre-recombinase is expressed. Expression of Emx1 is restricted to cortical pyramidal neurons (Chan et al., 2001) and starts from embryonic day 9.5 onwards. Thus, in contrast to previously reported studies, *Taok2* is only knocked out in pyramidal cells, making the *Taok2* (floxed/floxed) x Emx1-Cre KO mouse an exciting new model for the study of aberrant neuronal morphology and connectivity in the context of cognitive symptoms in schizophrenia.

1.3 Significance and objectives

This thesis aims to contribute to a better understanding of the cellular correlates of cognitive symptoms in schizophrenia. Furthermore, this thesis addresses the current lack of effective treatment of cognitive impairments, intending to identify novel treatment approaches and explore their specific mode of action. To achieve this, I investigated the function and structure of L5 neurons in acute slices of the PL of the mPFC in the *Neurod6* and the *Taok2* x Emx1-Cre KO mouse using whole-cell patch-clamp recordings and 2-photon imaging. In the former mouse model, L5 neurons were also subjected to pharmacological treatment, and in the latter mouse model, I compared results obtained from acute slices to *in vitro* results from primary cortical neurons.

In the first part of this thesis, I will focus on the *Neurod6* KO mouse, shedding light on the following questions:

Research question 1.1

Are there electrophysiological phenotypes in PL L5 neurons accompanying behavioral hyperactivity and increased impulsivity (Fig. **1.2.A)**?

Research question 1.2

If yes, is a selective pharmacological rescue of electrophysiological phenotypes via paliperidone and protriptyline possible, paralleling the rescue of behavioral hyperactivity and impulsivity (Fig. **1.2.B**)?

Research question 1.3

If yes, what is the specific mode of action of effective pharmacological compounds?

In the second part of this thesis, I will move on to the *Taok2* x Emx1-Cre KO mouse, focusing on the following questions:

Research question 2.1

Is the morphological complexity and circuit integration of PL L5 neurons disturbed?

Research question 2.2

Is the morphological complexity of primary cortical neurons in culture disturbed?

2 Materials

2.1 Equipment

2.1.1 Acute brain slice preparation

Equipment	Supplier, catalog number
Scissors	Fine Science Tools GmbH, Germany, 14001-14
2x Dumont #5 Forceps	Fine Science Tools GmbH, Germany, 11251-10
Standard Pattern Forceps	Fine Science Tools GmbH, Germany, 11000-12
Dumont #7 Forceps	Fine Science Tools GmbH, Germany, 11271-30
Spatula, 7mm	Hammacher, Germany, HSN 038-18
Spatula, 7mm, bent	Hammacher, Germany, HSN 038-18
Scalpel handle	Bayha GmbH, Germany, 502
Scalpel blades	neoLab, Germany, 1-1559
Ever-sharp-blades	Apollo Herkenrath, Germany, 10-102-055
Double edge coated blade	Electron Microscopy Sciences, USA, 72000-WA
Brush	daVinci Junior Synthetics, Germany, Series 303-1
Vibratome	Leica, Germany, VT1200S
Filter paper	Whatman, neoLab, Germany, VL-0160
2x slice incubation chambers	Custom-made
Glass coverslips, round, Ø: 12 mm, thickness: 0.13 mm	Roth, Germany, P231.1

Table 2.1 Equipment for acute brain slice preparation.

2.1.2 Electrophysiology and 2-photon imaging in acute slices and in vitro

Equipment	Supplier, catalog/model number
Upright microscope	Olympus, Japan, BX51WI
LUMPlan x60, 0.9 NA water immersion objective	Olympus, Japan
UMPlanFL x20, 0.5 NA water immersion objective	Olympus, Japan
PlanN x4, 0.1 NA air objective	Olympus, Japan
Video camera	Optronis, Germany, VX45

Table 2.2 Technical equipment for electrophysiology and imaging in acute slices and *in vitro*, cont. on p. 11.

Equipment	Supplier, catalog/model number
MaiTai HP DeepSee Ti:Sapphire laser	Spectra-Physics/Newport, USA, Mai Tai 10 S/N5123
Electro-optical modulator	Conoptics, USA, 350-80
Amplifier for electro-optical modulator	Conoptics, USA, 302RM
2x mechanical shutter	Uniblitz Vincent Associates, USA, VMM-D1
2x shutter driver	Uniblitz Vincent Associates, USA, VCM-D1
2x Low-Noise Current Preamplifier	Stanford Research Systems, USA, SR570
2x Photomultiplier Tube with D-type socket assembly	Hamamatsu, Japan, with E850-13
SM-5 9	Luigs & Neumann GmbH, Germany, 083-S90733
SM-5 Remote control system	Luigs & Neumann GmbH, Germany, 755-T0737
SM-5 Handwheel Cube	Luigs & Neumann GmbH, Germany, 139-CR0720
Micromanipulator	Luigs & Neumann GmbH, Germany, Junior ZL 10C100031
Axon MultiClamp 700B Amplifier with CV-7B headstage	Molecular Devices, USA, MULTICLAMP 700B
Micropipette Puller	Narishige, UK, PC-100
Thin wall capillaries	World Precision Instruments, USA, TW150F-3
Peristaltic pump	Gilson, USA, M312
Recording chamber	Custom-made
Dish holder	Custom-made
3.5 cm cell culture dish	Eppendorf, Germany, 0030 700.112

Table 2.2 Technical equipment for electrophysiology and imaging in acute slices and *in vitro*.

Software	Developer
MultiClamp 700B Commander	Molecular Devices, USA
LabVIEW 2017	National Instruments, USA

Table 2.3 Acquisition software for electrophysiology and imaging in acute slices and *in vitro*.

2.1.3 Analysis software

Software	Developer
ImageJ/Fiji	Wayne Rasband, National Institute of Health, USA
MATLAB Version R2021b	The MathWorks Inc., Natick, USA
R	R Core Team, Austria

Table 2.4 Analysis software.

2.2 Chemicals/Reagents

Chemical/Reagent	Supplier, catalog number
Alexa 594	Invitrogen, USA, A10438
Alexa 488	Invitrogen, USA, A10436
KCl(liq)	SIGMA, USA, 60135
KCl	SIGMA, USA, P5405
$CaCl_2$(liq)	SIGMA, USA, 21115
$MgCl_2$(liq)	SIGMA, USA, M1028
D-glucose (monohydrate)	Roth, Germany, 6887.1
Sucrose	Merck, Germany, 1.07651
NaCl	Roth, Germany, 3957.1
NaH_2PO_4 (monohydrate)	Merck, Germany, 3090
$NaHCO_3$	Honeywell Fluka, USA, 71630
Na_2HPO_4	Merck, Germany, 1.06586
DMSO	SIGMA, USA, D4500
HEPES	SIGMA, USA, H4034
K-gluconate	SIGMA, USA, G4500
$CsMeSO_4$	SIGMA, USA, C1426
Mg-ATP	SIGMA, USA, A9187
Na-GTP	SIGMA, USA, G8877
Na_2-phosphocreatine (monohydrate)	SIGMA, USA, P7936
EGTA	TOCRIS, UK, 2807

Table 2.5 Chemicals and reagents, cont. on p. 13.

Chemical/Reagent	Supplier, catalog number
Na-L-ascorbate	SIGMA, USA, 11140
Aqua B. Braun	B. Braun, Germany, 0082423E
Ethanol 80%, denatured (1% MEK, Iso+Bitrex)	Apotheke Großhadern, Germany
Carbogen (95% (vol/vol) O2, 5% (vol/vol) CO2)	Linde, Germany, 3 236 8747 10/20
$FeCl_3$ hexahydrate	Merck, Germany, 31232
Neurobasal medium	Gibco, USA, 21103049
B27 Supplement	Gibco, USA, 17504044
Glutamax	Gibco, USA, 35050038

Table 2.5 Chemicals and reagents.

2.3 Drugs

Drug	Supplier, catalog number
QX-314 Cl	TOCRIS, UK, 2313
TTX citrate	BIOTREND, Germany, BN0518
Paliperidone	Biosynth, UK, FP26725
Protriptyline hydrochloride	SIGMA, USA, P8813
DPO-1	TOCRIS, UK, 2533

Table 2.6 Drugs.

2.4 Buffers, solutions, and culture media

aCSF

NaCl, 127 mM; KCl, 2.5 mM; $NaHCO_3$, 25 mM; NaH_2PO_4, 1.25 mM; D-glucose (monohydrate), 25 mM; $CaCl_2$, 2 mM; $MgCl_2$, 1 mM; dissolved in distilled H_2O, pH = 7.35 - 7.45, 300 mOsm. A stock without $CaCl_2$ and $MgCl_2$ was prepared no more than 2 weeks in advance before patch-clamp recordings.

TTX (dissolved in distilled H_2O) was added to the solution at a concentration of 1 µM for recordings of mEPSCs and mIPSCs in *Taok2* KO neurons in the absence of action potentials.

Paliperidone (dissolved in DMSO), protriptyline (dissolved in distilled H_2O), or DPO-1 (dissolved in DMSO) was added to the solution at a concentration of 3.3 µM, 3.3 µM or 330 nM, and 30 nM, respectively, for pharmacological experiments in *Neurod6* KO neurons. The final DMSO concentration in aCSF containing paliperidone or DPO-1 was 0.04 % or 0.002 %, respectively.

Sucrose Cutting Solution

NaCl, 85 mM; Sucrose, 75 mM; D-glucose (monohydrate), 23 mM; KCl, 2.5 mM; $NaHCO_3$, 24 mM; NaH_2PO_4, 1.25 mM; $CaCl_2$, 0.5 mM; $MgCl_2$, 4 mM; dissolved in distilled H_2O, pH = 7.35 - 7.45, 310 - 325 mOsm. A stock without $CaCl_2$ and $MgCl_2$ was prepared no more than 1 day in advance before patch-clamp recordings.

K-gluconate internal solution

K-gluconate, 126 mM; KCl, 4 mM; HEPES, 10 mM; Mg-ATP, 4 mM; Na-GTP, 0.3 mM; Na_2-phosphocreatine, 10 mM; EGTA, 0.2 mM; dissolved in Aqua B. Braun, pH 7.25, 295 - 300 mOsm. The final solution containing Alexa 594 at a concentration of 0.03 mM was prepared from stocks (1 ml), filtered, aliquoted to ~20 µl, and stored at -20 °C.

Cs-methanesulfonate internal solution

$CsMeSO_4$, 122 mM; $MgCl_2$, 4 mM; HEPES, 10 mM; Mg-ATP, 4 mM; Na-GTP, 0.4 mM; Na_2-phosphocreatine, 10 mM; Na-L-ascorbate, 3 mM; EGTA, 0.2 mM; QX-314 Cl, 5 mM; dissolved in Aqua B. Braun, pH 7.25, 295 - 300 mOsm. The final solution containing Alexa594 at a concentration of 0.03 mM was prepared from stocks, filtered, aliquoted to ~20 µl, and stored at -20 °C.

This solution was used for recordings of mEPSCs and mIPSCs in the absence of action potentials.

Medium for primary cortical neuronal cultures

97 % Neurobasal medium, 2 % B27, 1 % Glutamax. The medium was freshly prepared on feeding days (by Wenbo Ma).

2.5 Mouse strains

Taok2 (floxed/floxed) x Emx1-Cre KO mice and *Taok2* (floxed/floxed) ctrl littermates were used for experiments regarding neuronal morphology in acute slices and primary neuronal culture.

Neurod6 full KO mice (-/-) with a C57Bl/6N-background and their wild-type littermates (*Neurod6* (+)) were used for experiments in acute slices investigating electrophysiological dysfunction accompanying behavioral phenotypes and their pharmacological rescue.

2.6 Viruses

To visualize the morphology of primary neurons in culture**,** AAV-hSynP-EGFP_DECr-shRNABC-DECf_SV40pA_shRNA_Scr1-hU6 (titer: 6.64 x 10^9 GC per µl + DNAse, plasmid cloned and packaged at the clinic by Vivek Sahoo) was used.

The virus was aliquoted (20 µl per aliquot), and aliquots were stored at -80 °C.

3 Methods

All experimental procedures were carried out in compliance with institutional guidelines of the BioMedical Center Munich, the LMU Clinic for Psychiatry and Psychotherapy Munich, and the local government (Regierung von Oberbayern).

3.1 Acute brain slice preparation

Before slice preparation, 500 ml of carbogenated cutting solution was cooled down to ~0°C until a slurry mix of frozen and liquid solution was obtained, and a custom-made incubation chamber was set up with 250 ml of continuously carbogenated cutting solution in a water bath at 35°C. To prepare acute coronal brain slices of the mPFC, animals were anesthetized with isoflurane in a sealed container (>100 mg/kg) or euthanized via cervical dislocation and decapitated with scissors. Both males and females were used for experiments. In *Neurod6* (-/-) and (+) mice, experiments were performed at P41-63. In *Taok2* (floxed/floxed) x Emx1-Cre-ko and *Taok2* (floxed/floxed) control mice, experiments were performed at P42-97, with one mouse being 139 days old. After decapitation, the head was placed into the ice-cold cutting solution, and skin and skull bone were cut open and removed using a scalpel and forceps. The brain was removed with a small spatula. The cerebellum and the rostral part of the brain were cut away coronally at an angle of ~30° aligned to the orientation of neurons in the prefrontal cortex. The brain was then glued – on the plane of the cut – onto a circular platform inside a cutting chamber, the chamber was filled with ice-cold continuously carbogenated cutting solution, and 300 µm thick coronal brain sections were cut with a vibratome. Brain slices including the mPFC started from ~300 µm behind the olfactory bulb and spanned a frontal-caudal range of ~1800 µm (Paxinos & Franklin, 2001) until the corpus callosum connecting the hemispheres was seen. The slices were transferred to the incubation chamber and incubated for 30 min to 1 hour. Afterward, the slices were kept in continuously carbogenated ACSF at room temperature for up to 9 h.

Malgorzata Frydrych helped prepare and maintain mPFC slices from *Neurod6* KO mice for pharmacological experiments under my guidance.

3.2 Whole-cell patch-clamp recordings of *Neurod6* KO and *Taok2* KO neurons

3.2.1 General procedure

Whole-cell patch-clamp recordings were performed on L5 neurons (300-600 µm from the pial surface, DeNardo, Berns, DeLoach, & Luo, 2015) in the PL of the mPFC in acute slices.

Before the start of a recording session, the exposed tip of the otherwise insulated silver electrode was chlorinated by incubating it for 5 min in $FeCl_3$. Borosilicate glass micropipettes with a resistance of 3 - 6 MOhm were pulled using a micropipette puller and filled with 3 µl of internal solution. The pipette was mounted on a Multiclamp 700B amplifier headstage fixed to a micromanipulator. The internal solution was either Cs-based when measuring mEPSCs and mIPSCs or K-based otherwise. For data acquisition, custom-written code in LabVIEW 2017 was used.

PL was identified according to coordinates derived from the mouse brain atlas (Paxinos & Franklin, 2001) using the midline as a reference. After recordings, a 2-photon image was taken with Laser-Dodt-contrast with a 4X air objective (1024 x 1024 pixels, 5.37 µm/pixel) to ascertain a neuron's correct localization in PL. Before entering the tissue, the voltage offset between bath and patch electrodes (liquid junction potential) was zeroed. Upon formation of a stable seal, a holding potential of -65 mV was applied. Data were acquired at a sampling rate of 10 kHz and digitally filtered at 4 or 3 kHz (Bessel filter). After a successful break-in, the values of series resistance, leak current, and bridge balance were monitored throughout the recording. If series resistance increased and stayed above 30 MOhm, leak current above +/-100 pA, resting potential above -50 mV, and/or bridge balance above 18 MOhm, cells were abandoned. Additionally, individual traces containing mEPSCs or mIPSCs not meeting the first two quality criteria were excluded, and a neuron was fully excluded from further analysis if its resting membrane potential changed by ≥ 20 % throughout the recording session. Capacitance compensation was applied.

Malgorzata Frydrych contributed to recordings in pharmacologically treated *Neurod6* KO neurons under my supervision.

3.2.2 Stimulation protocol and measured electrophysiological parameters for characterizing Neurod6 KO neurons

The protocol applied to characterize electrophysiological properties of *Neurod6* KO and ctrl neurons contained the following steps (**Fig. 3.1.A-D**):

1. Ramp: Neurons were stimulated ≥ 3 times with a 5 s - long depolarizing current of increasing intensity (25 pA/s), and action potentials were recorded.
2. Short square: Neurons were stimulated with 1, 2, or 3 ms - long current injections at +1000, +1500, or +2000 pA. Once a single action potential was elicited, the pulse was repeated ≥ 5 times. This step was skipped for treated KO neurons.
3. Long square hyperpolarizing: 1 s - long hyperpolarizing currents from -300 to -10 pA (in 100 pA increments from -300 to -100 pA, and 10 pA increments from -50 to -10 pA) were injected and the change in membrane voltage from the resting potential was recorded. Each current was applied ≥ 2 times. For treated KO neurons, only -200, -100, -50 and -10 pA were injected.
4. Long square depolarizing: Neurons were stimulated with a constant 1 s - long depolarizing above-threshold current from +100 to +500 pA (in 100 pA increments) and action potential trains were recorded. Each current was applied ≥ 2 times.

Electrophysiological parameters were extracted using custom-written software in MATLAB. Average values for all parameters across repetitions are reported.

Action potential threshold, rheobase, and resting membrane potential were calculated from the first action potential elicited by the ramping pulse and before stimulation, respectively (Step 1, **Fig. 3.1.A**).

1. Action potential threshold (mV): Membrane voltage at 5 % of the maximum rate of change of membrane voltage
2. Rheobase (pA): Current at the time the action potential threshold was reached
3. Resting membrane potential (mV): Average membrane potential over a period of 250 ms at rest, recorded 250 ms before stimulation and 1 - 2 min after break-in

Action potential waveform was analyzed from single action potentials in response to short square pulses (Step 2, **Fig. 3.1.B**) extracting the following parameters.

4. Action potential rise time (ms): Time from the maximum rate of change of the slope to the peak amplitude. The peak amplitude was defined as the maximum value of the trace (in mV).
5. Action potential half-width (ms): Width of the action potential at half its height. An action potential's half-height was defined as half the height (in mV) between threshold and peak.

6. Fast afterhyperpolarization (mV): Difference in membrane voltage between the action potential threshold value and the minimum value of the trace up to 5 ms after the peak (in mV). Action potential threshold was defined as the average value of membrane voltage during a timeframe of 0.2 ms before the maximum rate of change of the slope.

Input resistance was calculated from peak membrane voltage deflections from the resting membrane potential following the long square hyperpolarizing pulses (Step 3, **Fig. 3.1.C**).

7. Input resistance (MΩ): Estimated by the slope of the linear fit to the ΔV-I curve across all hyperpolarizing currents. ΔV was defined as the peak membrane voltage deflection from rest.

Number of action potentials and action potential train characteristics were calculated from trains of action potentials elicited by the long square depolarizing pulses (Step 4, **Fig. 3.1.D**). An action potential was defined as any response that reached an amplitude of above +10 mV. Frequently, the waveform of the last action potential in a train was not fully captured before the end of the pulse; thus, it was excluded from the analysis of train characteristics.

8. Number of action potentials: Number of action potentials per injected current

Action potential train characteristics included the following parameters:

9. First action potential amplitude (mV): First maximum value of the trace (absolute)
10. Last action potential amplitudes (mV): Average value of the second to last and third to last maximum values of the trace (absolute)
11. Repolarization (mV): Minimum value of the trace in between two subsequent action potential peaks relative to Vm rest, averaged across all pairs of peaks
12. Basal depolarization level (mV):

    In neurons with repetitive discharge during the last 300 ms of the pulse: Average value of the trace between the minimum after an action potential and the threshold of the subsequent action potential, calculated across the last three minimum-to-threshold pairs (absolute).

    In neurons without repetitive discharge during the last 300 ms of the pulse: Average value of the trace during the last 100 ms of the pulse (absolute).

    Basal depolarization level was calculated for all current injections from +100 pA to +500 pA resulting in up to five data points per neuron. To perform this analysis accurately, it was necessary to lower the amplitude threshold for action potential detection to -8 mV.

Malgorzata Frydrych contributed to the analysis of recordings in pharmacologically treated *Neurod6* KO neurons under my supervision.

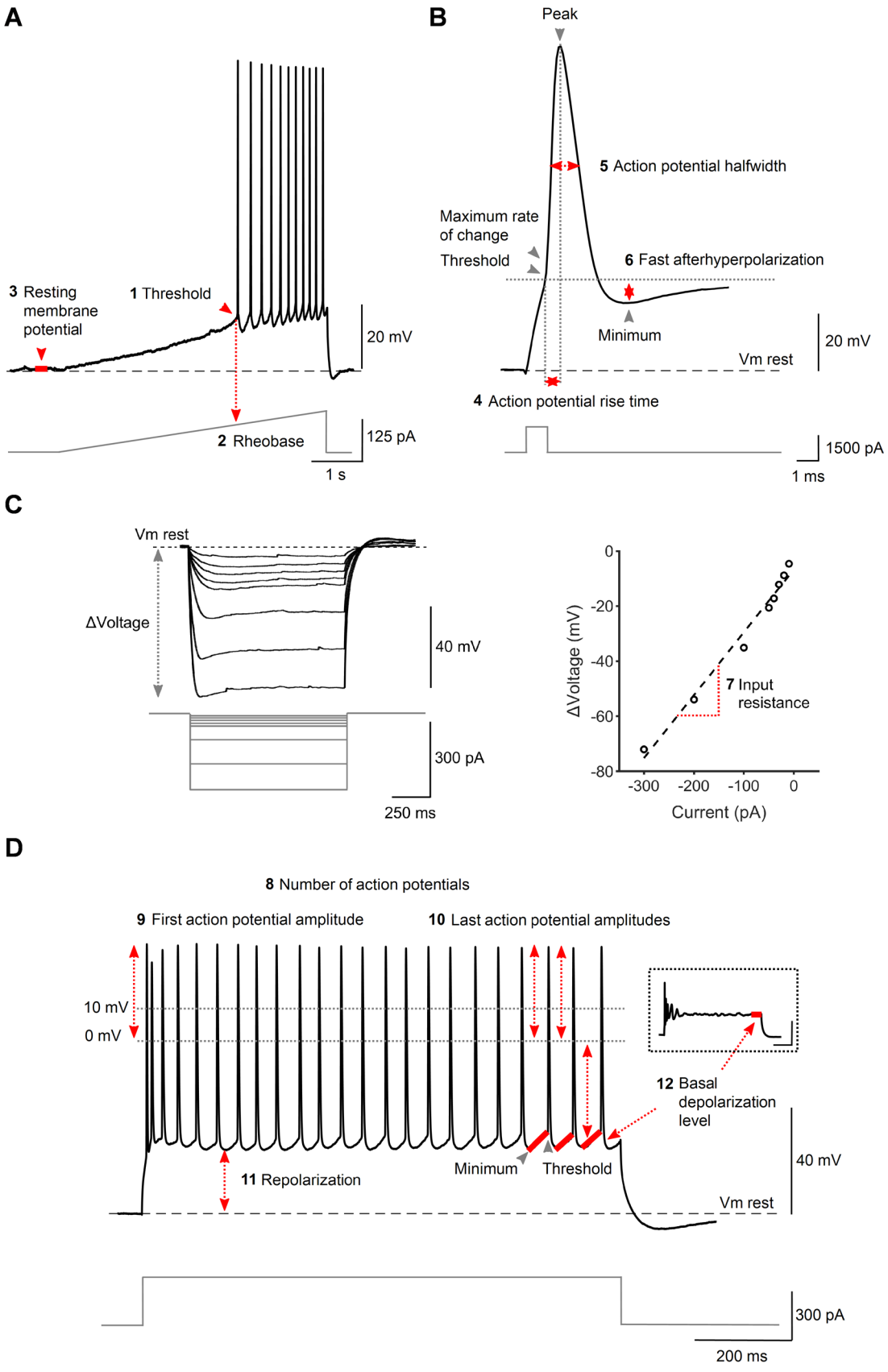
A
3 Resting membrane potential
1 Threshold
20 mV
2 Rheobase
125 pA
1 s
B
Peak
5 Action potential halfwidth
Maximum rate of change
Threshold
6 Fast afterhyperpolarization
Minimum
Vm rest
20 mV
4 Action potential rise time
1500 pA
1 ms
C
Vm rest
ΔVoltage
40 mV
300 pA
250 ms
ΔVoltage (mV)
0
-20
-40
-60
-80
-300
-200
-100
0
Current (pA)
7 Input resistance
D
8 Number of action potentials
9 First action potential amplitude
10 Last action potential amplitudes
10 mV
0 mV
12 Basal depolarization level
11 Repolarization
Minimum
Threshold
40 mV
Vm rest
300 pA
200 ms

Figure 3.1 Stimulation protocol and measured electrophysiological parameters in *Neurod6* KO.
A. Example trace for action potentials in response to a depolarizing current of increasing intensity (step 1). Extracted parameters are marked by red arrows and indicated with numbers. Red bar, resting membrane potential. Dashed line, Vm rest. **B.** Example action potential in response to a current of +1500 pA (step 3). Extracted parameters are marked by red arrows and indicated with numbers. Dashed line, Vm rest. **C.** Left, example traces for membrane voltage deflections (ΔVoltage, grey arrow) from Vm rest (dashed line) in response to hyperpolarizing current injections (step 2). Right, ΔV-I curve. Dashed line, linear fit to the ΔV-I curve, dotted red lines, slope of the linear fit. Empty circles, voltage deflection means per injected current. **D.** Example action potential trains for a neuron with and a neuron without (dotted inset) repetitive discharge in response to a depolarizing current injection of +300 pA (step 4). Extracted parameters are marked by red arrows and indicated with numbers. Lower horizontal dotted grey line, 0 mV. Upper horizontal dotted grey line, 10 mV. Red bars, basal depolarization level. Dashed line, Vm rest.

3.2.3 Voltage-clamp protocol and measured electrophysiological parameters for investigating circuit integration of Taok2 KO neurons

The protocol applied to investigate single-quantum synaptic inputs onto *Taok2* KO and ctrl neurons contained two steps (**Fig. 3.2**):

1. mEPSCs were recorded at a holding potential of -70 mV (≥ 60 s per neuron, 10 s per sweep).
2. mIPSCs were recorded at a holding potential of -35 mV (≥ 60 s per neuron, 10 s per sweep).

Neurons were clamped at -70 or -35 mV, respectively, during the entire time frame of recordings, and were only held at rest (-65 mV) after enough sweeps per condition had been acquired.

Electrophysiological parameters were extracted using custom-written software in MATLAB. mEPSC/mIPSC frequencies (**Fig. 3.2)** are reported based on the entire time frame of recordings.

1. mEPSC frequency (Hz): Frequency of spontaneous excitatory postsynaptic currents evoked by transmitter discharge from a single vesicle (single-quantum) in the absence of action potentials
2. mIPSC frequency (Hz): Frequency of spontaneous inhibitory postsynaptic currents evoked by transmitter discharge from a single vesicle (single-quantum) in the absence of action potentials

An exemplary template for postsynaptic current waveforms was used to detect mEPSCs and mIPSCs. This template was calculated for each neuron individually as the average of all potential postsynaptic current waveforms surpassing a certain amplitude threshold in an example trace. The amplitude threshold was manually adapted to the standard deviation of noise in the trace and ranged from +10 to +20 pA for mIPSCs and from -10 to -20 pA for mEPSCs. Subsequently, potential postsynaptic

currents in all traces were matched to the template and recognized as mEPSCs or mIPSCs based on a similarity criterion. In the next step, detected postsynaptic currents with an amplitude ≥ 12 pA were pre-selected. After manual confirmation, their frequency was calculated. Neurons with an average standard deviation of noise > 6 pA across traces were excluded, and individual traces of included neurons with a standard deviation of noise > 6 pA were excluded from analysis as well.

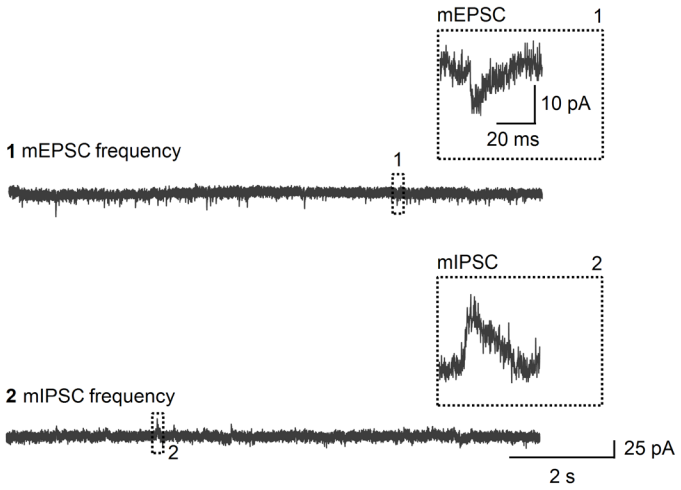

Figure 3.2 Voltage-clamp sweeps and measured electrophysiological parameters in *Taok2* KO.
Top, example trace containing mEPSCs acquired at a clamping voltage of -70 mV. Bottom, example trace containing mIPSCs acquired at a clamping voltage of -35 mV. Example traces are 10 s long corresponding to the length of one single sweep. Extracted parameters are indicated with numbers. The dotted boxes labelled 1 and 2 correspond to the dotted insets 1 and 2 on the right, showing a representative mEPSCs and a representative mIPSC, respectively.

3.3 Primary neuronal cultures

Primary neuronal cultures were prepared at embryonic day 15 from *Taok2* (floxed/floxed) x Emx1-Cre KO mice and *Taok2* (floxed/floxed) control mice by Wenbo Ma or Beate Kauschat. Neurons were grown in 3.5 cm dishes without coverslips and maintained by Wenbo Ma. On DIV0, neurons were infected by Wenbo Ma, using AAV-hSynP-EGFP_DECr-shRNABC-DECf_SV40pA_shRNA_Scr1-hU6 at an MOI of 1000 following an in-suspension transduction protocol developed by Vivek Sahoo and adapted by Wenbo Ma and myself. In short, 250 infected neurons were co-plated on DIV0 with 500000 not infected neurons per dish to keep overlap between eGFP-expressing neurons at a minimum. Co-plated infected and not infected cells were of the same genotype.

3.4 2-photon structural imaging of *Taok2* KO neurons

3.4.1 Image acquisition for analysis

Dendritic protrusions of neurons in acute slices of the PL of the mPFC

To detect and subsequently quantify basal and apical dendritic protrusions (spines and filopodia), two-photon image z-stacks capturing the entire spatial extent of basal and apical dendritic segments in z-direction were acquired. Images were taken after electrophysiological recordings to allow for a uniform fill of all morphological structures with Alexa594. Imaging of dendritic segments was performed at λ = 810 nm excitation wavelength with a 60X water-immersion objective (0.5 µm z increments, 512 x 512 pixels, 0.09 µm/pixel). Dendritic segments were excluded from analysis if signs of blebbing were present or if fluorescence was not bright enough.

Dendritic arbor of neurons in acute slices of the PL of the mPFC

After individual dendritic segments had been imaged, additional two-photon image z-stacks capturing the entire spatial extent of a neuron's dendritic arbor in z-direction were acquired. Imaging was performed at λ = 810 nm excitation wavelength with a 20X water-immersion objective (1 µm z increments, 1024 x 1024 pixels, 0.88 µm/pixel). If signs of blebbing were present, if fluorescence was not bright enough, and/or if invasion of dendrites from other neurons prevented unambiguous assignment of dendrites, the neuron was excluded from analysis.

Dendritic arbor and soma surface area of primary neurons in culture

Live primary neurons were imaged at DIV14/18 (KO) and DIV15/19 (ctrl) in 3.5 cm culture dishes mounted on a custom-made dish holder. During imaging, they were kept in culture medium. As dendrites of primary neurons were not as brightly labelled as those of neurons in the PL (see above), several two-photon image z-stacks had to be taken at a higher magnification to cover the neuron's extent in xy-direction, making sure to also include the soma. Imaging was performed at λ = 930 nm excitation wavelength with a 60X water-immersion objective (1 µm z increments, 1024 x 1024 pixels, 0.26 µm/pixel). If signs of blebbing were present, if fluorescence was not bright enough, and/or if invasion of dendrites from other neurons prevented unambiguous assignment of dendrites, the neuron was excluded from analysis.

3.4.2 Image analysis and morphological parameters

Images were analyzed and morphological parameters were extracted using ImageJ and the open-source TREES toolbox (Cuntz, Forstner, Borst, & Hausser, 2011) in MATLAB. PL Neurons in which the apical dendrite was cut due to the slicing procedure were included for analysis of basal morphology only.

Spine densities and the fraction of filopodia/protrusions are reported based on all analyzed dendritic segments (**Fig. 3.3.A**). Per neuron and dendritic subtree (basal and apical), ≥ 2 individual segments were analyzed, and the total length of analyzed segments per neuron and dendritic subtree was ≥ 90 µm (133.2 µm on average). Protrusions were counted along the entire length of dendritic segments in 3D in ImageJ on the recorded z-stacks using the cell counter plug-in. Spines were not classified into subtypes.

1. Apical spines/µm: Number of apical spines per µm
2. Basal spines/µm: Number of basal spines per µm
3. Apical filopodia/protrusions (%): Fraction of apical filopodia among all apical protrusions.
4. Basal filopodia/protrusions (%): Fraction of basal filopodia among all basal protrusions.

A neuron's dendritic arbor was traced manually using the Simple Neurite Tracer Plug-in in ImageJ. Before the dendritic arbor of primary neurons was traced, the individual image stacks per neuron were stitched together using the Stitching Plug-in in ImageJ. Stitching and tracings were performed by me, and Wenbo Ma and Yun Wai Foo helped with the tracings of 5 out of 35 primary neurons. Subsequently, morphological parameters 5 – 8 were extracted using the TREES toolbox (Cuntz et al., 2011). For PL-neurons, these parameters were extracted for basal and apical subtrees separately. For primary neurons, they were extracted for the entire dendritic tree, as the distinction between basal and apical subtrees was ambiguous.

5. Number of intersections: Number of dendritic intersections that occur at fixed distances from the soma center point in concentric circles (shells), starting with a radius of r = 25 µm and increasing by 25 µm each (Sholl analysis)
6. Number of branchpoints: Sum of all nodes in the dendritic arbor
7. Number of primary dendrites: Number of dendrites of first branch order, i.e. dendrites leaving the soma before the first branchpoint
8. Total cable length (µm): Summed up length of all dendritic sub-branches

Soma surface area is only reported for primary neurons with available data about dendritic arborization.

9. 2D soma surface area (μm^2): Soma surface area was calculated in ImageJ as 2D surface area on maximum intensity projections of the stitched z-stacks using the freehand selection and the measure tool.

Parameters 5 - 9 are visualized in Fig. **3.3.B**, taking a primary neuron as an example.

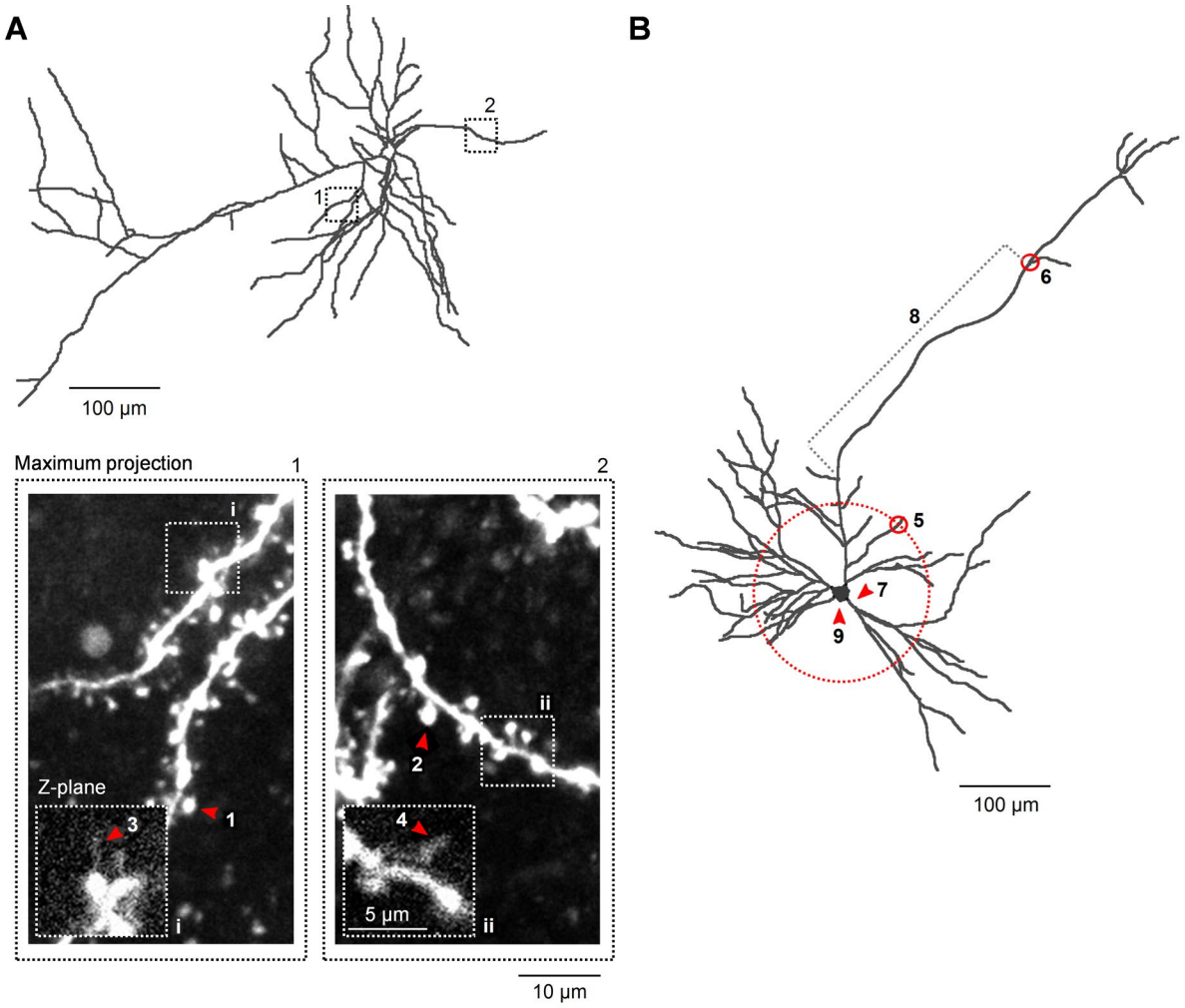

Figure 3.3 Extracted morphological parameters in *Taok2* KO.

A. Top, example PL-neuron, oriented towards the pial surface on the left. The dotted boxes labelled 1 and 2 correspond to the dotted insets 1 and 2 below. Bottom, insets show maximum intensity z-projection zoom-ins of two apical segments(1) and one basal segment (2). The dotted boxes labelled i and ii correspond to the dotted insets i and ii, showing a single z-plane with filopodia at the site enclosed by the box. Note: Structures shown in maximum intensity projections and individual z-planes may differ due to the fact that maximum projections are 2D projections of all z-planes. Extracted parameters are marked by red arrows and indicated with numbers. 1, apical dendritic spines/µm, 2, basal dendritic spines/µm, 3, apical filopodia/protrusions, 4, basal filopodia/protrusions. **B.** Example primary neuron. Extracted parameters are marked by red arrows and/or indicated with numbers. 5, number of intersections, dotted red circle, example shell with r = 100 µm, red circle, one marked intersection, 6, number of branchpoints, red circle, one marked branchpoint, 7, number of primary dendrites, 8, total cable length, dotted grey lines denote a sub-branch, 9, 2D soma surface area.

3.5 Statistics

Data are reported as mean ± s.e.m.. Before statistical analyses, data sets were checked for normality and variance homogeneity using the Shapiro-Wilk or the Lilliefors test and the Levene test, respectively. Two-tailed *t*-tests or mixed ANOVA were performed if requirements were met, and data sets with at least one group lacking normality or with at least one group showing $n < 10$ were compared using nonparametric equivalents (two-tailed Wilcoxon rank-sum test or Kruskal-Wallis-test). Multiple comparisons were taken into account by using the Bonferroni correction. Data sets for linear regression models were checked for normality and conditional homoscedasticity of residuals using the Lilliefors and the Engle's ARCH test, respectively. Significance values are indicated as follows: #, $P < .1$ *, $P < .05$, **, $P < .01$, ***, $P < .001$, ****, $P < .0001$, *n.s.*, not significant.

4 Results

4.1 *Neurod6* KO leads to impaired electrophysiological functioning in L5 neurons of the PL that can be rescued pharmacologically

4.1.1 Neurod6 KO neurons are hyperexcitable and show a disturbed use-dependent action potential generation

Using whole-cell patch-clamp recordings, I explored the electrophysiological function of L5 principal neurons in the PL of the mPFC (Fig. **4.1.1.A**). First, I investigated passive membrane properties. KO neurons reacted with stronger membrane voltage deflections from Vm rest to 1 s - long hyperpolarizing current injections than ctrl neurons: Input resistance was significantly increased in KO (ctrl = 146.1 ± 7.3 MΩ; KO = 182.9 ± 10.7 MΩ; P = .009; t-test, two-tailed; Fig. **4.1.1.B-C**). Taking this a step further, I probed the reaction of KO and ctrl neurons to a 5 s - long current injection of increasing intensity (25 pA/s) to determine rheobase and action potential threshold. KO neurons fired action potentials (Fig. **4.1.1.D**), and their action potential threshold was not significantly different from ctrls (ctrl = -41.8 ± 0.87 mV; KO = -40.0 mV ± 1.1 mV; P = .22; t-test, two-tailed, Fig. **4.1.1.E**). However, in line with an increased input resistance, this threshold was reached at lower currents for KO neurons (ctrl = 61.9 ± 4.2 pA; KO = 47.6 ± 4.0 pA; P = .016; t-test, two-tailed; Fig. **4.1.1.F**). In conclusion, these findings reveal *Neurod6* KO neurons to be hyperexcitable compared to wild-type controls.

There was no influence of *Neurod6* KO on single action potential shape. Rise time (ctrl = 0.83 ± 0.027 ms; KO = 0.81 ± 0.015 ms; P = .46; t-test, two-tailed), half-width (ctrl = 1.7 ± 0.068 ms; KO = 1.7 ± 0.033 ms; P = .10; Wilcoxon rank-sum test, two-tailed), and fast afterhyperpolarization (ctrl = 8.1 ± 1.6 mV; KO = 5.4 ± 1.3 mV; P = .20; t-test, two-tailed) were indistinguishable between ctrl and KO. Resting membrane potential was similar for ctrl and KO as well (ctrl = -70.8 ± 1.3 mV; KO = -69.1 ± 1.3 mV; P = .34; t-test, two-tailed; Supplementary fig. **6.1.1.A-E**).

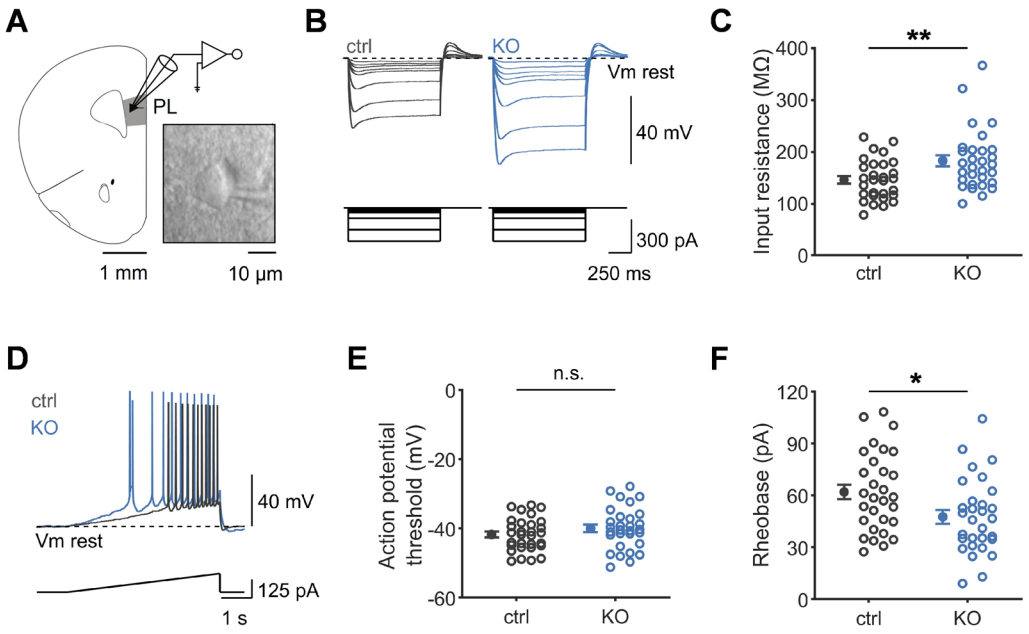

Figure 4.1.1 *Neurod6* KO neurons are hyperexcitable.

A. Whole-cell patch-clamp recordings were performed on L5 ctrl and KO neurons in the PL of the mPFC. Schematic taken from Paxinos and Franklin (2001) and modified, +1.98 mm from Bregma. **B.** Example traces for membrane voltage deflections from Vm rest (dashed line) in response to hyperpolarizing current injections. **C.** The input resistance in KO neurons (n = 30) was significantly increased compared to ctrl (*n* = 29), *P* = .009. **D.** Example traces for action potentials in response to a depolarizing current of increasing intensity. Dashed line, Vm rest. **E, F.** Action potential threshold did not differ significantly between ctrl (*n* = 30) and KO neurons (*n* = 30), *P* = .22, but KO neurons displayed a significantly decreased rheobase, *P* = .016.

t-tests (two-tailed). Filled circles and error bars, means ± s.e.m, empty circles, individual neuron data.

Next, I explored firing patterns of KO and ctrl neurons in response to 1s - long depolarizing above-threshold currents (Fig. **4.1.2.A**). Interestingly, action potential numbers at current injections of +300, +400, and +500 pA were reduced in KO (+300 pA: ctrl = 18.8 ± 1.1; KO = 13.0 ± 1.8; *P* = .030; +400 pA: ctrl = 21.3 ± 1.1; KO = 12.6 ± 1.9; *P* = 8.9 x 10^{-4}; +500 pA: ctrl = 21.6 ± 1.5; KO = 9.7 ± 2.0; *P* = 8.2 x 10^{-5}; Bonferroni-corrected post-hoc-tests after significant interaction, *P* = 2.7 x 10^{-8}, in mixed ANOVA; Fig. **4.1.2.B,** left panel). When looking at the data for individual neurons, it is evident that several KO neurons fired similarly to ctrls. However, 13 out of 25 KO neurons, i.e. 52 %, fired fewer action potentials at +300, +400, or +500 pA current injections than 2 SD below the ctrl mean. These neurons are referred to as "phenotypic neurons" (Fig. **4.1.2.B,** right panel; Fig. **4.1.4.D**).

Furthermore, the last action potential amplitudes in an action potential train decreased significantly in KO with increasing current intensity, but not in ctrl (*P* = 9.9 x 10^{-4}; Bonferroni-corrected

post-hoc-tests after significant interaction, *P* = .010, in mixed ANOVA). The difference between ctrl and KO reached significance at a current injection of +400 pA (ctrl = 32.3 ± 1.4 mV; KO = 24.3 ± 1.9 mV; *P* = .008; Bonferroni-corrected post-hoc-test). The first action potentials, however, reached a similar amplitude (ctrl = 41.2 ± 1.7 mV; KO = 42.0 ± 1.7 mV*; P* = .74; *t*-test, two-tailed; Fig. **4.1.2.C-D**). Additionally, in an action potential train, the lower the last action potential amplitudes were, the fewer action potentials were fired (*P* = .003; linear regression; Supplementary fig. **6.1.2**, right panel).

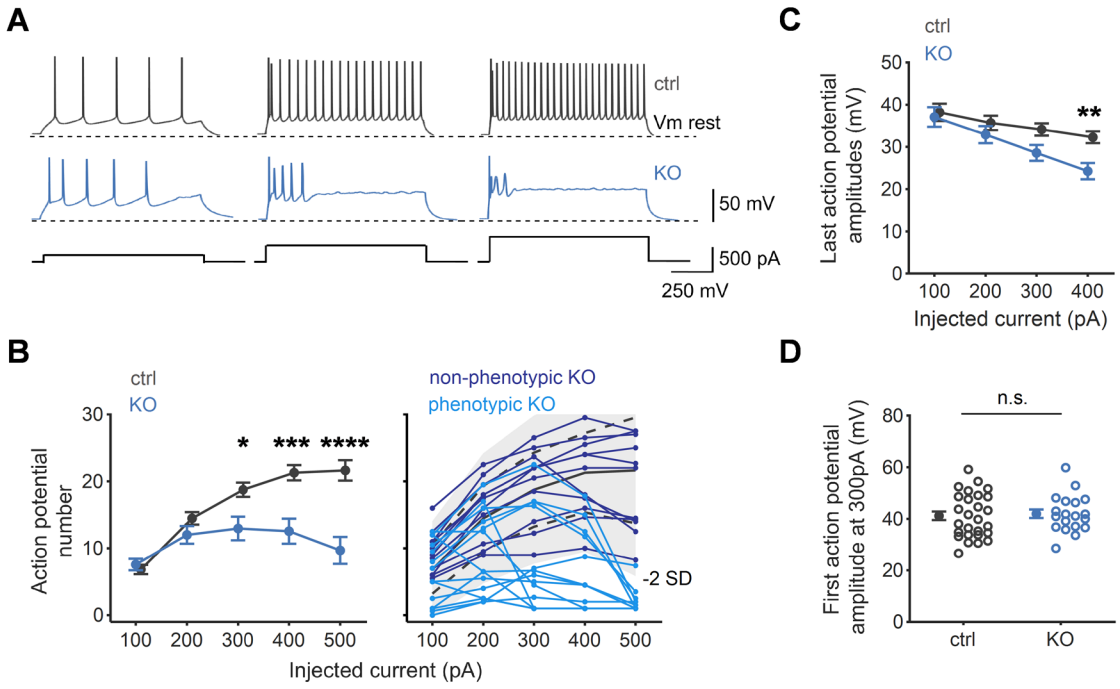

Figure 4.1.2 *Neurod6* KO neurons show a disturbed use-dependent action potential generation.

A. Example traces for action potential trains in response to a depolarizing above-threshold current injection (+100 pA, left, +300 pA, middle, +500 pA, right). Dashed line, Vm rest. **B.** Left, at +300, +400, and +500 pA current injections, KO neurons (*n* = 25) fired significantly fewer action potentials than ctrl neurons (*n* = 27), *P* = .030, $P = 8.9 \times 10^{-4}$, and $P = 8.2 \times 10^{-5}$, respectively. Right, 13 out of 25 KO neurons, i.e. 52 %, fired fewer action potentials at +300, +400, or +500 pA current injections than 2 SD below the ctrl mean (= phenotypic neurons). Black line, ctrl mean, dashed lines, ctrl mean ± 1 SD, grey area, area marking ± 2 SD around ctrl mean. **C.** At a current injection of +400 pA, the amplitudes of the last action potentials in a train were significantly decreased in KO (*n* = 11) compared to ctrl (*n* = 20), *P* = .008. Amplitudes at a current injection of +500 pA were not included due to insufficient number of data points. **D.** The amplitude of the first action potential was similar in ctrl (*n* = 27) and KO neurons (*n* = 19), *P* = .74. Results are shown for an exemplary current injection of +300 pA.

Mixed ANOVA and post-hoc-tests (Bonferroni-corrected), *t*-test (two-tailed). Filled circles and error bars, means ± s.e.m, empty circles, individual neuron data.

In conclusion, use-dependent action potential generation of KO neurons was disturbed at higher current intensities.

Interestingly, hyperexcitability and disturbed use-dependent action potential generation depended on one another: Input resistance was negatively correlated with action potential number (P = .029; linear regression; Supplementary fig. **6.1.2**, left panel).

Hypothesizing that the drop in action potential number in phenotypic KO neurons could be due to overstimulation resulting from a higher input resistance, I compared the level of basal depolarization between phenotypic and non-phenotypic KO neurons and ctrl neurons. Indeed, phenotypic KO neurons showed an increased level of basal depolarization compared to both other groups (phenotypic KO = -32.2 ± 1.4 mV; non-phenotypic KO = -42.0 ± 1.3 mV; $P = 3.5 \times 10^{-7}$; ctrl = -40.4 ± 0.76 mV; $P = 1.8 \times 10^{-7}$; Bonferroni-corrected post-hoc-tests after significant group effect, $P = 1.0 \times 10^{-8}$, in one-way ANOVA; Fig. **4.1.3.A**). Additionally, the level of basal depolarization was positively correlated with action potential number in ctrl and non-phenotypic KO neurons. In contrast, action potential number decreased with increasing basal depolarization level in phenotypic KO neurons (ctrl: $P = 3.3 \times 10^{-4}$; non-phenotypic KO: P = .033; phenotypic KO: $P = 4.1 \times 10^{-4}$; linear regressions). It is noteworthy that the highest levels of basal depolarization were reached by phenotypic KO neurons with a low number of action potentials only. However, several phenotypic KO neurons with a low number of action potentials reached similar levels of basal depolarization as both non-phenotypic KO neurons and ctrl neurons with sustained repetitive discharge (Fig. **4.1.3.B**).

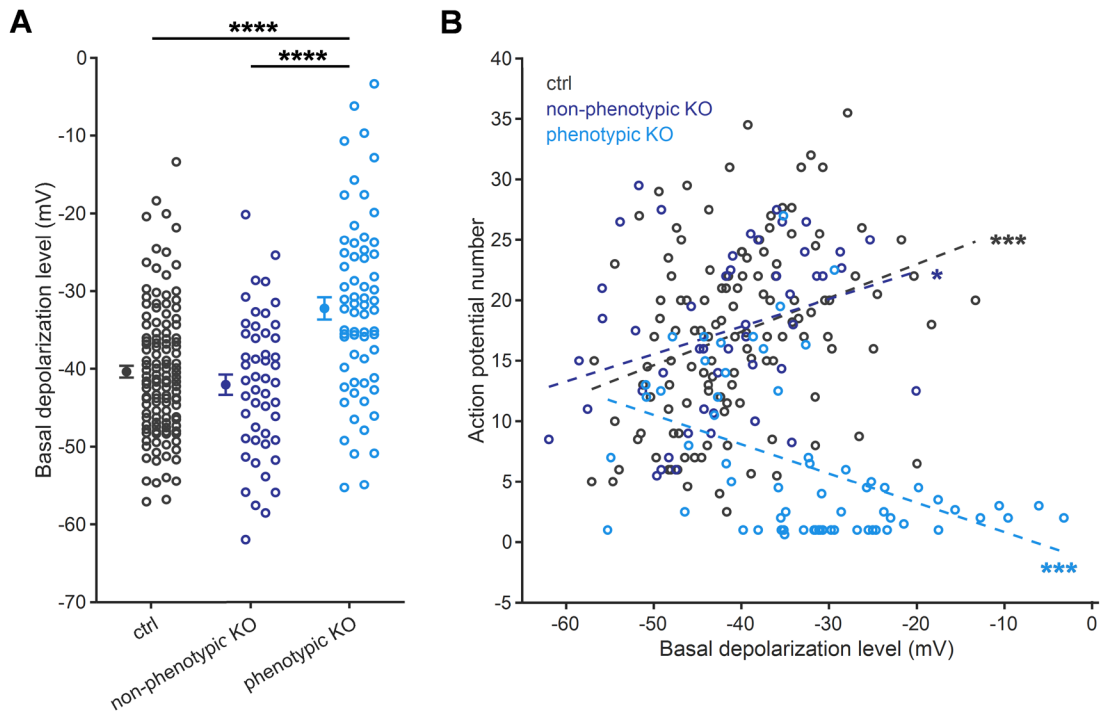

Figure 4.1.3 The level of basal depolarization is higher and negatively correlated with action potential number in phenotypic KO.

A. Phenotypic KO neurons (n = 64) showed a significantly higher level of basal depolarization than non-phenotypic KO neurons (n = 49) and ctrl neurons (n = 124), $P = 3.5 \times 10^{-7}$, and $P = 1.8 \times 10^{-7}$, respectively. **B.** In ctrl (n = 124) and non-phenotypic KO neurons (n = 49), action potential number increased with increasing basal depolarization level, $P = 3.3 \times 10^{-4}$, R^2 = .10, and P = .033, R^2 = .093, respectively. In phenotypic KO neurons (n = 64), action potential number decreased with increasing basal depolarization level, $P = 4.1 \times 10^{-4}$, R^2 = .18.

One-way ANOVA and post-hoc-tests (Bonferroni-corrected), linear regressions. Filled circles and bars, means ± s.e.m, empty circles, individual neuron data. Dashed lines, linear fits.

4.1.2 Use-dependent action potential generation can be rescued by protriptyline and DPO-1

Next, I tested the effects of protriptyline and paliperidone on the phenotypes described in Fig. **4.1.1-2**. In separate experiments, both compounds were directly added to aCSF, and neurons had been exposed to them for at least one hour before recordings. In the case of protriptyline, a conservative concentration of 330nM was chosen. From dose-response curves generated by colleagues at the clinic using online reporter assays of neuronal activity in cultured primary neurons, this concentration was estimated to show a small effect. Due to the fact that paliperidone was 5 to 10 times less potent than protriptyline, a 10-fold higher concentration of 3.3 µM was chosen for paliperidone.

At current injections of +400 and +500 pA, paliperidone-treated KO neurons – like untreated KO neurons – fired significantly fewer action potentials than ctrl neurons (+400 pA: paliperidone-treated KO = 13.0 ± 2.0*; P* = .001; +500 pA: paliperidone-treated KO = 9.4 ± 2.0; $P = 3.1 \times 10^{-5}$; Bonferroni-corrected post-hoc-tests after significant interaction, $P = 2.6 \times 10^{-8}$, in mixed ANOVA). The average number of action potentials at any given current injection was indistinguishable from untreated KO neurons (Fig. **4.1.4.B**, top left panel, Fig. **4.1.4.A**, top row). 9 out of 20 paliperidone-treated KO neurons, i.e. 45 %, were classified as phenotypic neurons (Fig. **4.1.4.B**, top right panel; Fig. **4.1.4.D**). This ratio is very likely if the probability of phenotypic neurons was the same as in untreated KO neurons (*P* = .41; binomial test, two-tailed).

In stark contrast, action potential numbers of protriptyline-treated KO neurons approached control levels. These neurons fired significantly more action potentials at +300 and +400 pA current injections than untreated KO neurons (+300 pA: protriptyline-treated KO = 18.8 ± 1.1; *P* = .027; +400 pA: protriptyline-treated KO = 19.1 ± 1.8*; P* = .049; Bonferroni-corrected post-hoc-tests after significant interaction, $P = 6.2 \times 10^{-5}$, in mixed ANOVA; Fig. **4.1.4.B**, middle left panel, Fig. **4.1.4.A**, middle row). Additionally, only 5 out of 22 protriptyline-treated KO neurons, i.e. 22.7 %, were classified as phenotypic neurons (Fig. **4.1.4.B**, middle right panel; Fig. **4.1.4.D**). This ratio would be very unlikely if the probability of phenotypic neurons were the same as in untreated KO neurons (*P* = .009; binomial test, two-tailed).

The next step was to explore protriptyline's mode of action. As mentioned previously, protriptyline primarily acts as a serotonin and norepinephrine reuptake inhibitor. However, it has also been shown to block voltage-gated potassium channels of the Kv1.5 subtype in rabbit heart muscle cells (An et al., 2020). These channels conduct the ultra-rapid delayed rectifier current contributing to action potential repolarization, and inhibition of voltage-gated potassium channels was demonstrated to increase repetitive firing rate (Agren, Nilsson, & Arhem, 2019; Cramer, Stagnitto, Knowles, & Palmer, 1994; Kocsis, Eng, Gordon, & Waxman, 1987; Rho, Szot, Tempel, & Schwartzkroin, 1999; Voskuyl & Albus, 1985). To confirm the hypothesis that blocking the Kv1.5 channel subtype rescues repetitive firing in *Neurod6* KO neurons, I performed recordings in the presence of DPO-1, a selective blocker of Kv1.5 channels (Du et al., 2010). DPO-1 was directly added to aCSF, and neurons had been exposed to the compound for at least one hour before recordings. From the dose-response curve in An et al. (2020), it was estimated that ~10 % of Kv1.5 channels should be inhibited by 330 nM protriptyline. Thus, I aimed for a similar percentage of inhibition with DPO-1. Using the dose-response curve in Du et al. (2010), I decided on a concentration of 30 nM, corresponding to ~20 % inhibition.

Strikingly, action potential firing patterns of DPO-1-treated KO neurons were very similar to those observed under the application of protriptyline. Action potential numbers of DPO-1-treated KO neurons were indistinguishable from ctrl levels. DPO-1-treated KO neurons fired significantly more action potentials at +300, +400, and +500 pA current injections than untreated KO neurons (+300 pA: DPO-1-treated KO = 20.6 ± 1.1; P = .003; +400 pA: DPO-1-treated KO = 19.5 ± 2.0; P = .044; +500 pA: DPO-1-treated KO = 18.0 ± 2.3; P = .028; Bonferroni-corrected post-hoc-tests after significant interaction, $P = 2.9 \times 10^{-5}$, in mixed ANOVA; Fig. **4.1.4.B**, bottom left panel, Fig. **4.1.4.A**, bottom row). In contrast to untreated KO neurons, only 6 out of 21 DPO-1-treated KO neurons, i.e. 28.6 %, were classified as phenotypic neurons (Fig. **4.1.4.B**, bottom right panel; Fig. **4.1.4.D**). As for protriptyline-treated KO neurons, this ratio would be very unlikely if the probability of phenotypic neurons were the same as in untreated KO neurons (P = .013; binomial test, two-tailed).

Consistent with the hypothesis that protriptyline acts via blocking Kv1.5 channels, the last action potential amplitudes in an action potential train of protriptyline- and DPO-1-treated KO neurons were similar to ctrl, even at +400 pA current injections (+400 pA: protriptyline-treated KO = 29.7 ± 2.3 mV; P = 1; DPO-1-treated KO = 30.3 ± 2.2 mV; P = .95; Bonferroni-corrected post-hoc-tests after significant interaction, P = .008, in mixed ANOVA; Fig**. 4.1.4.C**).

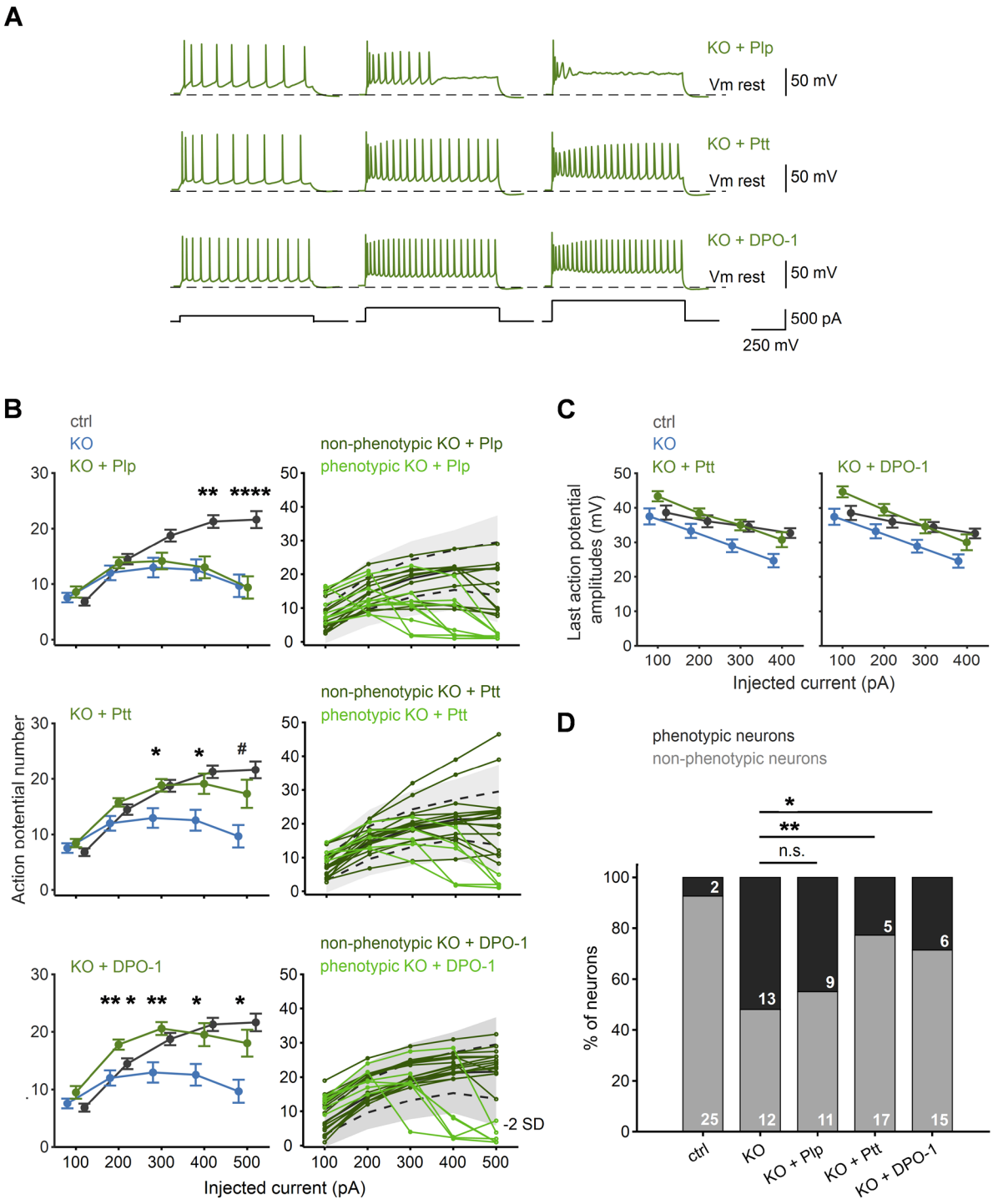
A
KO + Plp
Vm rest
50 mV
KO + Ptt
Vm rest
50 mV
KO + DPO-1
Vm rest
50 mV
500 pA
250 mV
B
ctrl
KO
KO + Plp
non-phenotypic KO + Plp
phenotypic KO + Plp
KO + Ptt
non-phenotypic KO + Ptt
phenotypic KO + Ptt
KO + DPO-1
non-phenotypic KO + DPO-1
phenotypic KO + DPO-1
-2 SD
Action potential number
Injected current (pA)
C
ctrl
KO
KO + Ptt
KO + DPO-1
Last action potential amplitudes (mV)
Injected current (pA)
D
phenotypic neurons
non-phenotypic neurons
n.s.
% of neurons
ctrl
KO
KO + Plp
KO + Ptt
KO + DPO-1

Figure 4.1.4 Protriptyline and DPO-1, but not paliperidone, rescue use-dependent action potential generation. **A.** Example traces for action potential trains in response to a depolarizing above-threshold current injection (+100 pA, left column, +300 pA, middle column, +500 pA, right column) in treated KO neurons (paliperidone-treated, top row, protriptyline-treated, middle row, DPO-1-treated, bottom row). Dashed lines, Vm rest. **B.** Top left, paliperidone-treated KO neurons (*n* = 20) fired a similar number of action potentials as untreated KO neurons (*n* = 25), and significantly less action potentials at +400 and +500 pA current injections than ctrl neurons (*n* = 27), *P* = .001 and *P* = 3.1 x 10^{-5}, respectively. Top right, similar to untreated KO neurons, 9 out of 20 paliperidone-treated KO neurons, i.e. 45 %, fired fewer action potentials at +300, +400, or +500 pA current injections than 2 SD below the ctrl mean (= phenotypic neurons). Middle left, protriptyline-treated KO neurons (*n* = 22) fired a similar number of action potentials as ctrl neurons (*n* = 27), and significantly more action potentials at +300 and +400 pA current injections than untreated KO neurons (*n* = 25), *P* = .027 and *P* = .049, respectively. Middle right, in contrast to untreated KO neurons, only 5 out of 22 protriptyline-treated KO neurons, i.e. 22.7 %, fired fewer action potentials at +300, +400, or +500 pA current injections than 2 SD below the ctrl mean (= phenotypic neurons). Bottom left, DPO-1-treated KO neurons (*n* = 21) behaved similarly to protriptyline-treated KO neurons. They fired a similar number of action potentials as ctrl neurons (*n* = 27), and significantly more action potentials at +300, +400, and +500 pA current injections than untreated KO neurons (*n* = 25), *P* = .003, *P* = .044, and *P* = .028, respectively. Additionally, they fired significantly more action potentials at a current injection of +200 pA than ctrl and KO neurons, *P* = .046 and *P* = .003, respectively. Bottom right, in contrast to untreated KO neurons, only 6 out of 21 DPO-1-treated KO neurons, i.e. 28.6 %, fired fewer action potentials at +300, +400, or +500 pA current injections than 2 SD below the ctrl mean (= phenotypic neurons). Black line, ctrl mean, dashed lines, ctrl mean ± 1 SD, grey area, area marking ± 2 SD around ctrl mean. Ctrl and KO data as shown in Fig. **4.1.2.B.** **C.** The last action potential amplitudes of protriptyline (*n* = 13, left) - or DPO-1 (*n* = 12, right) - treated KO neurons in a train were indistinguishable from ctrls (*n* = 20) at a current injection of +400 pA, *P* = 1, and *P* = .95, respectively. KO, *n* = 11. ctrl and KO data as shown in Fig. **4.1.2.C. D.** Percentage of phenotypic and non-phenotypic neurons in ctrl, KO, paliperidone-treated KO, protriptyline-treated KO, and DPO-1-treated KO. Numbers inside bars indicate the absolute number of neurons. Phenotypic neurons were less likely to occur in protriptyline- and DPO-1-treated KO neurons than in untreated KO neurons, *P* = .009, and *P* = .013, respectively. However, the probability of occurrence of phenotypic neurons was indistinguishable between paliperidone-treated and untreated KO, *P* = .41.

Plp, paliperidone, *Ptt*, protriptyline. Mixed ANOVA and post-hoc-tests (Bonferroni-corrected), binomial tests (two-tailed). Filled circles and bars, means ± s.e.m, empty circles, individual neuron data.

More evidence supporting this hypothesis comes from preliminary experiments in which neurons were treated with 3.3 µM protriptyline, 10 times the concentration used in the experiments mentioned above, expected to inhibit ~30 % of Kv1.5 (An et al., 2020). Again, protriptyline was directly added to aCSF, and neurons had been exposed to the compound for at least one hour before

recordings. With a concentration of 3.3 µM, action potential numbers at +300, +400, and +500 pA current injections dropped even further (Fig. **4.1.5.A**, left panel). More importantly, and in contrast to untreated KO neurons, 10 out of 11 protriptyline-treated KO neurons, i.e. 90.9 %, were classified as phenotypic neurons (Fig. **4.1.5.A**, right panel). This ratio would be very unlikely if the probability of phenotypic neurons were the same as in untreated KO neurons (P = .008; binomial test, two-tailed). Furthermore, the amplitudes of the last action potentials decreased compared to untreated KO neurons (KO = 27.9 ± 1.5 mV; protriptyline-treated KO = 20.4 ± 1.9 mV; P = .015; Wilcoxon rank-sum test, two-tailed; Fig. **4.1.5.B**). Treated KO neurons lost their ability to repolarize (KO = 24.4 ± 1.6 mV; protriptyline-treated KO = 31.2 ± 2.1 mV; P = .036; t-test, two-tailed; Fig. **4.1.5.C**).

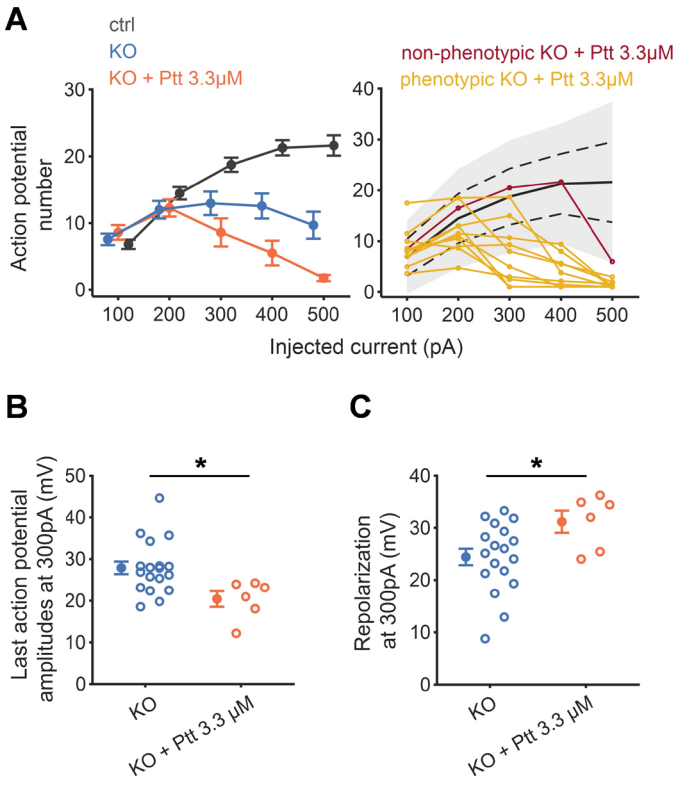

Figure 4.1.5 A higher concentration of protriptyline is detrimental to repetitive action potential firing.

A. Left, action potential numbers of protriptyline-treated KO neurons (n = 11), untreated KO neurons (n = 25), and ctrl neurons (n = 27) at current injections from +100 to +500 pA. Right, in contrast to untreated KO neurons, 10 out of 11, i.e., 90.9 % of protriptyline-treated KO neurons fired fewer action potentials at +300, +400, or +500 pA current injections than 2 SD below the ctrl mean (= phenotypic neurons). Black line, ctrl mean, dashed lines, ctrl mean ± 1 SD, grey area, area marking ± 2 SD around ctrl mean. Ctrl and KO data as shown in Fig. **4.1.2.B**. **B.** The last action potential amplitudes of protriptyline-treated KO neurons (n = 6) in a train were significantly

lower than those of untreated KO neurons (*n* = 18), *P* = .015. **C.** Protriptyline-treated KO neurons (*n* = 6) repolarize less than untreated KO neurons (*n* = 18), *P* = .036. In **B** and **C**, Results are shown for a current injection of +300 pA because the number of data points for protriptyline-treated KO neurons was insufficient at higher current injections.

Ptt, protriptyline. Wilcoxon rank-sum tests (two-tailed). Filled circles and bars, means ± s.e.m, empty circles, individual neuron data.

In summary, a low concentration of protriptyline and DPO-1, inhibiting 10 - 20 % of Kv1.5 channels, rescued action potential number and increased action potential amplitudes. A higher concentration of protriptyline, inhibiting ~30 % of Kv1.5 channels, was detrimental to repetitive firing. Together, these findings support the hypothesis that protriptyline acts via Kv1.5 in influencing repetitive firing capability.

Interestingly, even though hyperexcitability and use-dependent action potential generation seem linked (Supplementary fig. **6.1.2,** left panel), neither protriptyline or DPO-1 nor paliperidone rescued input resistance or rheobase, respectively (input resistance: protriptyline-treated KO = 176.3 ± 13.4 MΩ; DPO-1-treated KO = 173.2 ± 14.2 MΩ; paliperidone-treated KO = 173.7 ± 12.0 MΩ; *P* = .77; Kruskal-Wallis-test; rheobase: protriptyline-treated KO = 52.5 ± 6.0 pA; DPO-1-treated KO = 57.2 ± 6.4 pA; paliperidone-treated KO = 47.4 ± 5.7 pA; *P* = .53; one-way ANOVA; Supplementary fig. **6.1.3, A-B**).

To summarize, the application of protriptyline and DPO-1, but not of paliperidone, rescued use-dependent action potential generation, likely via blocking Kv1.5 channels. Neither compound rescued hyperexcitability.

4.2 Cre-conditional KO of *Taok2* does not affect L5 neurons of the PL but cultured primary cortical neurons

4.2.1 There is no effect of cre-conditional KO of Taok2 on the complexity of dendritic arborization, the spine density, or miniature synaptic currents in L5 neurons of the PL

Using 2-photon imaging and whole-cell patch-clamp recordings, I explored morphological complexity and synaptic integration of L5 principal neurons in the PL of the mPFC. First, I investigated the complexity of dendritic arborization (see Supplementary fig. **6.2.1** for an overview of all reconstructed morphologies). Basal and apical subtrees were analyzed separately (Fig. **4.2.1.A**).

Unexpectedly and contrary to the findings reported in the literature (see section 1.2.4), I could not confirm any alterations regarding the number of primary basal dendrites (ctrl = 6.0 ± 0.76; KO = 6.8 ± 0.52; *P* = .33; Wilcoxon rank-sum test, two-tailed; Fig. **4.2.1.B**). Sholl analysis revealed a similar number of basal intersections for ctrl and KO neurons (*P* = .27; mixed ANOVA; Fig. **4.2.1.C**, left panel). Basal spine density was unaltered as well (ctrl = 1.4 ± 0.14 spines/µm; KO = 1.3 ± 0.12 spines/µm; *P* = .53; Wilcoxon rank-sum test, two-tailed; Fig. **4.2.1.D-E**, left panel). In line with these findings, there was no significant difference regarding mEPSC or mIPSC frequency between ctrl and KO (mEPSC frequency: ctrl = 1.2 ± 0.41 Hz; KO = 0.81 ± 0.26 Hz; *P* = .82; mIPSC frequency: ctrl = 0.10 ± 0.090 Hz; KO = 0.22 ± 0.10 Hz; *P* = .28; Wilcoxon rank-sum tests, two-tailed; Fig. **4.2.1.F-G**). As previously reported, the number of apical intersections (Fig. **4.2.1.C**, right panel) and apical spine density in KO neurons were similar to ctrl (ctrl = 1.6 ± 0.11 spines/µm; KO = 1.6 ± 0.14 spines/µm; *P* = .76; Wilcoxon rank-sum test, two-tailed; Fig. **4.2.1.E**, right panel).

The number of filopodia was negligible in general, and neither the fraction of basal nor apical filopodia among the protrusions was significantly different between ctrl and KO (basal filopodia/protrusions: ctrl = 1.1 ± 0.57 %; KO = 1.0 ± 0.39 %; *P* = .98; apical filopodia/protrusions: ctrl = 0.58 ± 0.35 %; KO = 0.51 ± 0.17 %; *P* = 1; Wilcoxon rank-sum tests, two-tailed; Supplementary fig. **6.2.2**).

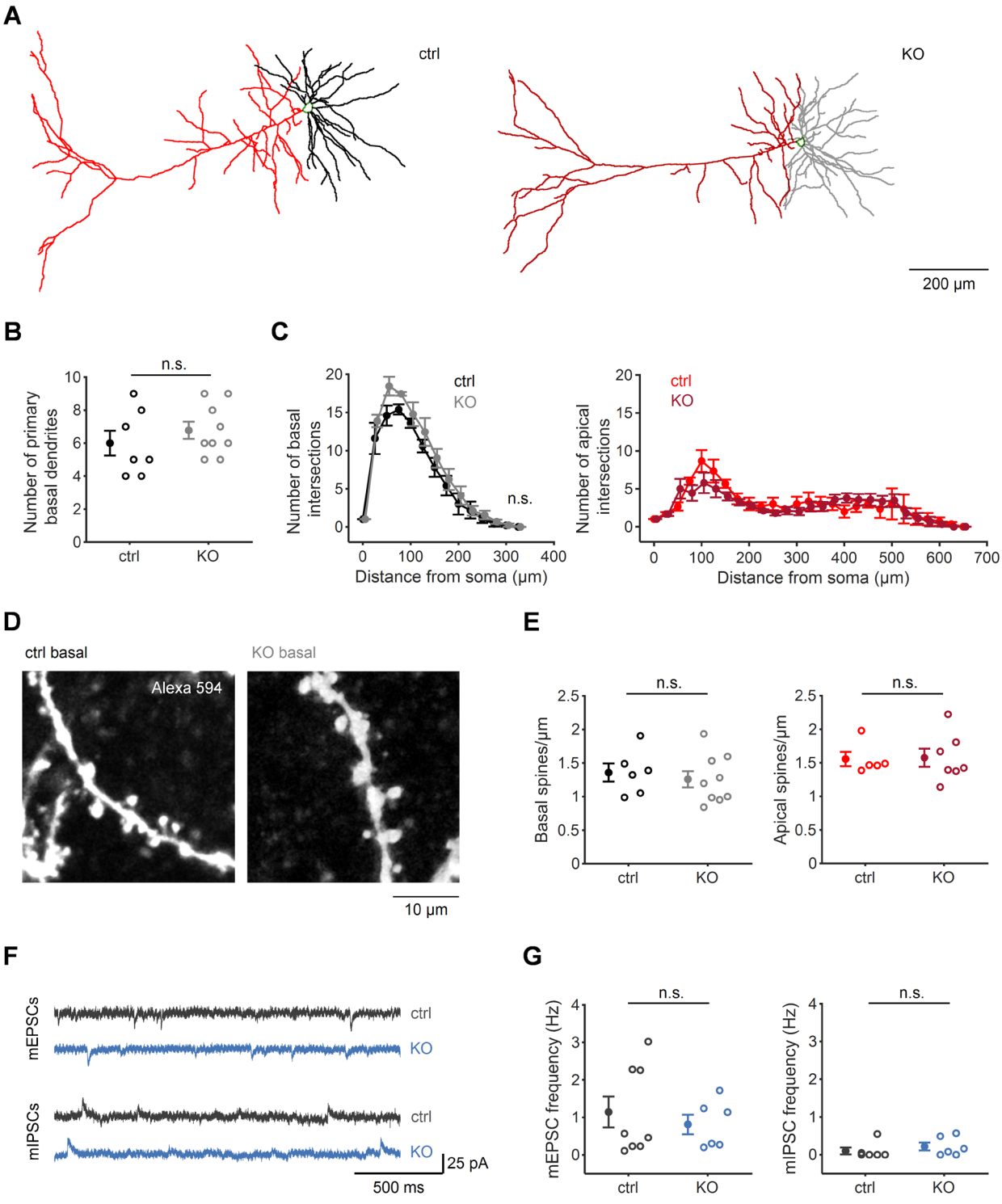
A
ctrl
KO
200 µm
B
n.s.
Number of primary basal dendrites
ctrl
KO
C
Number of basal intersections
ctrl
KO
n.s.
Distance from soma (µm)
Number of apical intersections
ctrl
KO
Distance from soma (µm)
D
ctrl basal
KO basal
Alexa 594
10 µm
E
n.s.
Basal spines/µm
Apical spines/µm
ctrl
KO
F
mEPSCs
mIPSCs
ctrl
KO
25 pA
500 ms
G
n.s.
mEPSC frequency (Hz)
mIPSC frequency (Hz)
ctrl
KO

Figure 4.2.1 Cre-conditional *Taok2* KO does not influence the complexity of dendritic arborization, the spine density, and miniature synaptic currents of PL L5 neurons in acute slices.

A. Example *Taok2* ctrl and KO neurons. Light red, apical dendritic tree in ctrl, dark red, apical dendritic tree in KO, black, basal dendritic tree in ctrl, grey, basal dendritic tree in KO, green, soma outline. Neurons oriented towards the pial surface on the left. **B.** The number of primary basal dendrites was not significantly different between ctrl (*n* = 7) and KO (*n* = 9), *P* = .33. **C.** Left, the number of basal intersections (Sholl analysis) was not significantly different between ctrl (*n* = 5) and KO (*n* = 9), P = .27. Right, number of apical intersections in ctrl (*n* = 3) and KO (*n* = 9). **D.** Example basal dendritic segments for ctrl and KO. **E.** Left, basal spine density was not significantly different between ctrl (*n* = 6) and KO (*n* = 9), P = .53. Right, apical spine density was not significantly different between ctrl (*n* = 5) and KO (*n* = 7), *P* = .76. **F.** Top, example traces containing mEPSCs acquired at a clamping voltage of -70 mV. Bottom, example traces containing mIPSCs acquired at a clamping voltage of -35 mV. **G.** Left, mEPSC frequency was not significantly different between ctrl (*n* = 8) and KO (*n* = 6), *P* = .82. Right, mIPSC frequency was not significantly different between ctrl (*n* = 6) and KO (*n* = 6), *P* = .28.

Mixed ANOVA, Wilcoxon rank-sum tests (two-tailed). Filled circles and bars, means ± s.e.m., empty circles, individual neuron data.

In summary, dendritic morphology and circuit integration were unaltered in *Taok2* KO PL L5 neurons.

Consequently, I decided to repeat experiments in cultured primary cortical neurons, hoping to shed light on the reasons for this apparent discrepancy between the data reported in this thesis and in the literature. Here, I examined the effects of *TAOK2* KO specifically on PL L5 neurons. Primary cortical neuronal cultures, however, include neurons from all cortical layers and various cortical areas (for a preparation protocol, see, e.g., Sahu, Nikkila, Lagas, Kolehmainen, & Castren, 2019), and data on neuronal morphology can more easily be obtained from cultures by, e.g., AAV-mediated expression of fluorescent proteins in infected neurons.

4.2.2 The complexity of dendritic arborization is reduced in primary neuronal cultures

Indeed, dendritic arborization in primary neuronal cultures was underdeveloped (Fig. **4.2.2**; see Supplementary fig. **6.2.3** for an overview of all reconstructed morphologies). There was a trend towards a lower number of primary dendrites in KO neurons compared to ctrl (ctrl = 9.8 ± 0.51; KO = 8.3 ± 0.72; *P* = .091; *t*-test, two-tailed; Fig. **4.2.2.B**), and Sholl analysis revealed a significantly lower number of intersections in KO neurons (*P* = .002, mixed ANOVA; Fig. **4.2.2.C**). Furthermore, the number of branchpoints and total cable length were significantly reduced (number of branchpoints: ctrl = 48.5 ± 2.9; KO = 38.6 ± 3.7; *P* = .038; total cable length: ctrl = 5425.0 ± 275.3 µm; KO = 4140.8 ± 307.2 µm; *P* = .004; *t*-tests, two-tailed; Fig. **4.2.2.D-E**). 2D soma surface area of KO neurons, however, was similar to ctrls (ctrl = 286.2 ± 17.2 μm^2; KO = 280.7 ± 25.1 μm^2; *P* = .83; Wilcoxon rank-sum test, two-tailed; Fig. **4.2.2.F**).

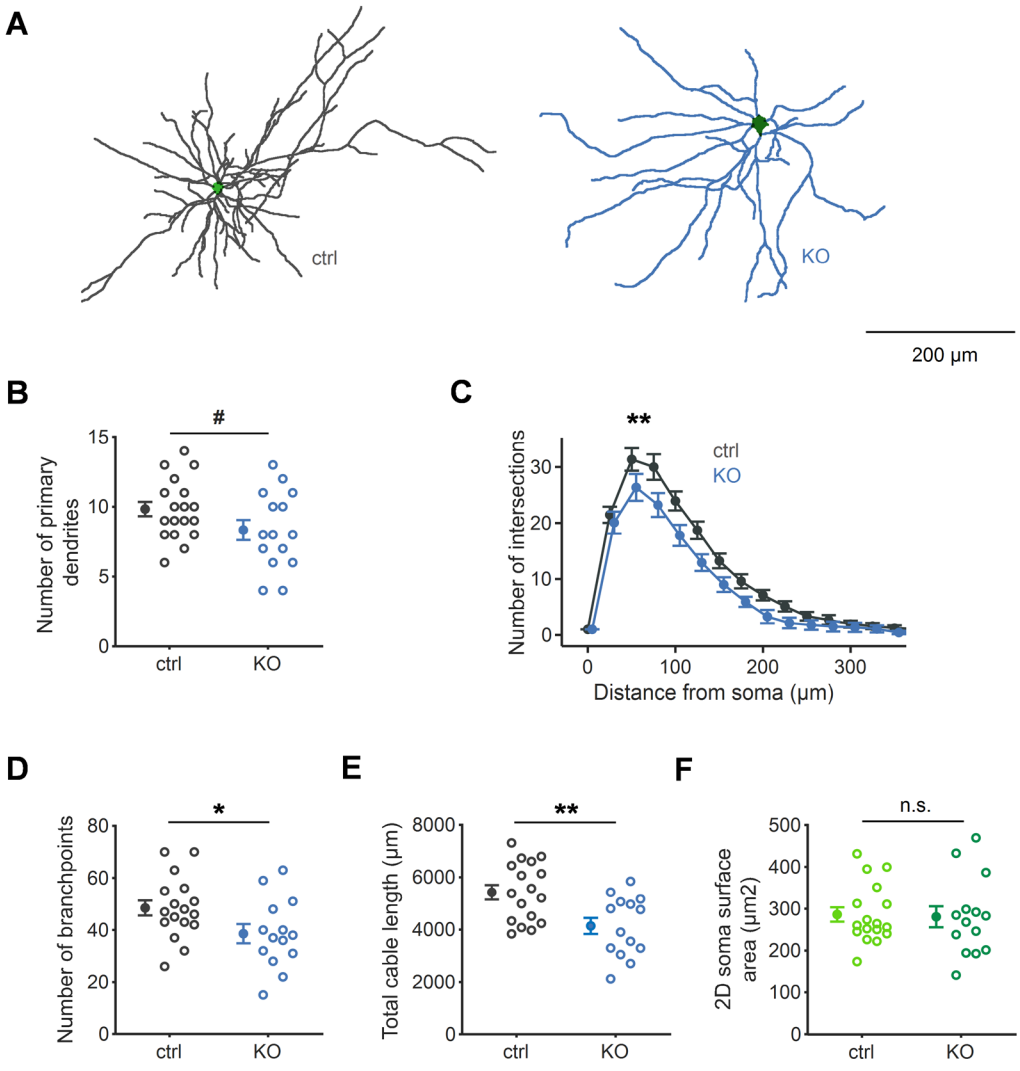

Figure 4.2.2 The complexity of dendritic arborization is reduced in cultured primary cortical *Taok2* KO neurons. **A.** Example *Taok2* ctrl and KO neurons. Light green, soma surface area in ctrl, dark green, soma surface area in KO. **B.** There was a trend towards fewer primary dendrites in KO (n = 15) compared to ctrl (n = 18), P = .091. **C.** KO neurons (n = 14) had a significantly lower number of intersections (Sholl analysis) than ctrl (n = 17), P = .002. **D.** The number of branchpoints was significantly lower in KO (n = 14) compared to ctrl (n = 17), P = .038. **E.** Total cable length was significantly lower in KO (n = 14) compared to ctrl (n = 17), P = .004. **F.** 2D soma surface area was not significantly different between ctrl (n = 17) and KO (n = 14), P = .83.
Mixed ANOVA, t-tests (two-tailed), and Wilcoxon rank-sum test (two-tailed). Filled circles and bars, means ± s.e.m., empty circles, individual neuron data.

In summary, even though no effect of cre-conditional *Taok2* KO on the morphological complexity of PL L5 neurons was observed, cultured primary cortical neurons were morphologically underdeveloped.

5 Discussion

In this thesis, I investigated cellular correlates of behavioral phenotypes in mouse models of schizophrenia, novel treatment approaches, and their mode of action. To this end, I used whole-cell patch-clamp recordings in acute cortical slices and 2-photon imaging of neuronal morphology in slices and primary cortical neuronal cultures.

5.1 *Neurod6* KO leads to impaired electrophysiological functioning in L5 neurons of the PL that can be rescued pharmacologically

In the first part of this thesis, I focused on the function of L5 neurons in acute slices of the PL of the mPFC in the *Neurod6* KO mouse, answering the following questions (see section 1.3):

Research question 1.1

Are there electrophysiological phenotypes in PL L5 neurons accompanying behavioral hyperactivity and increased impulsivity (Fig. **1.2.A)**?

Research question 1.2

Is selective pharmacological rescue of electrophysiological phenotypes via paliperidone and protriptyline possible, paralleling the rescue of behavioral hyperactivity and impulsivity (Fig. **1.2.B**)?

Research question 1.3

If yes, what is the specific mode of action of effective pharmacological compounds?

In conclusion, I identified electrophysiological dysfunction at the cellular level in *Neurod6* KO mice. L5 PL neurons of the mPFC were hyperexcitable, as evidenced by an increased input resistance and a lower rheobase, and showed a disturbed use-dependent action potential generation: Action potential numbers and the last action potential amplitudes at higher current intensities were reduced. Furthermore, sustained firing and action potential amplitudes could be rescued by applying protriptyline and DPO-1, but not paliperidone. Neither compound rescued hyperexcitability. A high concentration of protriptyline was detrimental to sustained firing, reducing action potential numbers and amplitudes even further and disturbing repolarization between action potentials. This points towards a common mode of action of protriptyline and DPO-1 – the blocking of Kv1.5 channels.

5.1.1 Increased input resistance as a key player in neuronal excitability

KO neurons were hyperexcitable: Less current was needed to reach action potential threshold (Fig. **4.1.1.F**). The action potential threshold is defined as a threshold voltage for the opening of voltage-gated sodium channels, subsequently driving the upstroke of an action potential. This opening occurs when depolarization activates all four charged S4 helices of the four domains that comprise a sodium channel. The helices are driven outwards, the channels' activation gate opens, and sodium influx occurs (Armstrong, 2006). The action potential threshold of KO neurons was indistinguishable from ctrl (Fig. **4.1.1.E**). Thus, the S4 helices are driven outwards at a similar potential difference between the inside and the outside of the neuron, reflecting a comparable level of voltage sensitivity. Accordingly, the enhanced excitability in KO neurons is due to an increased input resistance only (Fig. **4.1.1.C**).

An explanation for the increased input resistance is a reduced voltage-independent leak conductance of the neuronal membrane. Leak channels that are normally open at rest comprise sodium, potassium, and chloride channels. Major contributors to neuronal leak conductance are outwardly rectifying potassium channels, with a membrane permeability larger than that of chloride by a factor of 2 and larger than that of sodium by a factor of 25 - 40 (Henley, 2021). However, it is currently unclear how *Neurod6* KO affects leak conductance of the neuronal membrane. Furthermore, it is unclear whether a hypothesized reduced leak conductance is due to the involved channels being hypoconductive, possibly following conformational changes of one or more channel subunits affecting the pore (selectivity), or possibly due to a block. The reduced leak conductance may also be due to fewer channels on the membrane, or due to a combination of both less and hypoconductive channels. It is of note that Vm rest was similar in KO and ctrl (Supplementary fig. **6.1.1.E**). This makes it unlikely that the conductivity of only one channel type is affected. Due to the high membrane permeability for potassium, Vm rest is usually closer to the equilibrium potential of potassium (see, e.g., Ren, 2011). A lower conductance for potassium alone, for example, could drive Vm rest towards the equilibrium potential for sodium, i.e. towards more depolarized values. Compensatory mechanisms have to be at play, e.g., an increased conductivity for chloride ions. However, if either potassium or sodium channel conductivity is affected, concentration gradients might be less pronounced. Taking into account the similar first action potential amplitude in a train of action potentials and the overall similar action potential shape when firing only one action potential (Supplementary fig. **6.1.1.A-D**), the driving force for sodium and potassium ions to move across the membrane and channel kinetics seem to be comparable between KO and ctrl. Another possible explanation without compensatory conductance changes would be an altered activity of the sodium-potassium-ion pump to compensate for changes in

Vm rest. Hyperactivity of the pump moving sodium out of the cell could counteract a more depolarized Vm rest due to lower potassium channel conductivity. What makes this possibility unlikely is that an altered activity of the pump would lead to changes in ionic concentration as well, as would equally affected conductances for potassium and sodium channels. It could be possible that only chloride channels are affected, as chloride's influence on Vm rest is not as pronounced due to its reversal potential being very close to Vm rest. However, due to variations in chloride transporter expression across neurons and resulting variations in intracellular concentrations, this relationship can be complex (Ren, 2011). More experiments are needed, such as snRNAseq experiments, to explore channel expression levels.

An alternative explanation for an increased input resistance may be a decrease in soma surface area (see, e.g., Torres-Torrelo, Torres, & Carrascal, 2014). This parameter was not investigated in this thesis. However, other mouse models of schizophrenia present a reduced surface area of frontal cortical neurons (see, e.g., F. H. Lee et al., 2011), and a reduced surface area leading to higher input resistance was also observed in a mouse model of cognitive dysfunction in Alzheimer's disease (Arsenault, Julien, Tremblay, & Calon, 2011). Furthermore, the authors showed that agents rescuing surface area and input resistance also rescued cognitive dysfunction.

5.1.2 A depolarization block prevents KO neurons from sustained action potential firing

The present thesis also demonstrates a reduction in action potential numbers and the last action potential amplitudes at higher current intensities for KO neurons compared to ctrl (Fig. **4.1.2**.**B-C**). Gerstner, Kistler, Naud, and Paninski (2014) categorize neuronal firing patterns into several subclasses. One is the tonic or the adapting firing pattern, describing neurons that fire action potentials throughout the entire stimulation period, either with regularly spaced or with gradually increasing inter-spike times. Transient, or phasic, firing, on the other hand, describes neurons that fire only a few spikes and then remain silent, even if stimulation is maintained. This firing behavior is consistent with the low number of action potentials observed in some phenotypic KO neurons. However, phasic neurons tend to increase their spike numbers with increasing current intensity (usually remaining far below 10 spikes, L. Wang, Liang, Zhang, & Qiu, 2014). This does not accurately describe the firing behavior of the neurons in this study. In fact, most of the phenotypic KO neurons showed the opposite tendency: At lower current intensities, they fired few to several action potentials, but the numbers dropped with increasing current intensity (Fig. **4.1.2.B**, right panel**)**. This is more reminiscent of what has been described as a "depolarization block" in neurons with a tonic firing pattern (L. Wang et al., 2014): Neurons eventually stop firing under sustained input currents of increasing strength.

Bianchi et al. (2012) proposed a model on underlying mechanisms for such a depolarization block in hippocampal neurons involving voltage-gated sodium and delayed-rectifier potassium currents. In their models, a depolarization block could be achieved under the constraint of a right-shifted activation curve of potassium current compared to sodium, and a small sodium window current in the membrane potential range where steady-state sodium activation and inactivation overlap. The block seems to be caused by sodium channels not fully de-inactivating between spikes, together with a small activation of delayed-rectifier potassium current unable to repolarize the membrane. As a result, fewer and fewer sodium channels are available to generate full-amplitude action potentials. This model explains both the decreased number of action potentials and the decreased amplitudes of the last action potentials observed at higher current intensities (Fig. **4.1.2**.**B-C**). It is also consistent with the fact that, in an action potential train, the lower the last action potential amplitudes were, the fewer action potentials were fired (Supplementary fig. **6.1.2**, right panel). In Bianchi et al. (2012), the depolarization block becomes apparent mostly at current intensities above +600 pA, and the authors postulate input resistance as the determining factor for the threshold current to enter the block: The higher the input resistance, the lower the threshold current. As input resistance in KO neurons was significantly higher than in ctrl (Fig. **4.1.1.C**), it is plausible that they enter a depolarization block at lower current intensities. In this context, it is noteworthy that the number of action potentials could be predicted from the input resistance (Supplementary fig. **6.1.2**, left panel), demonstrating that the depolarization block was stronger in neurons with higher input resistance. Indeed, phenotypic KO neurons showed a higher level of basal depolarization across all current intensities compared to both ctrl and non-phenotypic KO neurons (Fig. **4.1.3.A**), hinting at a potential overstimulation. This hypothesis was strengthened by the fact that the highest levels of basal depolarization were reached by phenotypic KO neurons with a low number of action potentials only. However, there were several phenotypic KO neurons presenting a medium-to-high level of basal depolarization comparable to ctrls and non-phenotypic KO neurons. Whereas these phenotypic KO neurons already fired few action potentials, both other groups were still able to maintain repetitive discharge (Fig. **4.1.3.B**). Thus, it can be concluded that overstimulation due to a higher input resistance might only partially be accountable for the disturbed use-dependent action potential generation seen in KO neurons. A depolarization block in KO neurons without overstimulation might still be plausible hypothesizing a right-shifted activation curve of potassium current and a small sodium window current (see above). To confirm this hypothesis, it will be necessary to investigate potassium and sodium activation and inactivation (curves) in *Neurod6* KO neurons compared to ctrls.

It is important to note here that the depolarization block as a phenomenon has rarely been investigated, probably due to being considered unphysiological. However, Bianchi et al. (2012) found

that synaptic activity involving less than 3 % of the total number of excitatory synapses on CA1 neurons could easily be capable of generating currents around +1 nA, inducing a depolarization block. Furthermore, and most importantly, *Neurod6* KO PL neurons already started exhibiting this feature around a much lower current injection of +300 pA, whereas ctrl neurons were not affected, including current injections of up until +500 pA (Fig. **4.1.2.B**).

This has important implications. In a large network including the PL of the mPFC, several PL neurons would likely be in a depolarization block at any given time. Thus, their firing behavior would be opposite of that of unaffected neurons firing at high rates, disturbing network communication and, ultimately, leading to dysconnectivity hypothesized to be the root cause of schizophrenia (see section 1.1.3).

5.1.3 Protriptyline and DPO-1 block Kv1.5 channels leading to an increase in action potential firing

I have demonstrated that the tricyclic antidepressant protriptyline and the Kv1.5 blocker DPO-1 rescued both the number of action potentials and the last action potential amplitudes. The antipsychotic paliperidone had no effect (Fig. **4.1.4**).

The main mode of action for protriptyline is serotonin and norepinephrine reuptake inhibition, together with antagonizing histamine H1 receptors, muscarinic receptors, serotonin 2A receptors, and α1-adrenergic receptors (Leysen, Niemegeers, Van Nueten, & Laduron, 1982; Richelson & Nelson, 1984; Tatsumi, Groshan, Blakely, & Richelson, 1997; Tran, Chang, & Snyder, 1978; Warchal et al., 2020). A complete list of transporters, receptors, and binding affinities can be found in the Psychoactive Drug Screening Program Ki Database of the National Institute of Mental Health: https://pdsp.unc.edu/databases/kidb.php. Considering all of the above, protriptyline application leads to higher levels but decreased neurotransmission of serotonin and norepinephrine.

Interestingly, it was demonstrated that protriptyline also blocks voltage-gated potassium channels, mainly the ultra-rapid delayed rectifier current Kv1.5, in rabbit coronary arterial smooth muscle cells (An et al., 2020). The authors postulated a closed-state inhibition due to a change in inactivation gating properties, with channels being inactivated at lower voltages. Kv channels are involved in the repolarization phase after an action potential, and inhibition of Kv channels has been shown to increase repetitive firing rate, both in computational models (Agren et al., 2019) as well as across a range of channel blockers like 4-AP and TEA (Cramer et al., 1994; Kocsis et al., 1987; Rho et al., 1999; Voskuyl & Albus, 1985). In the case of 4-AP, it was shown that this effect is due to a lowered action potential threshold, quickening further action potential generation and inducing repetitive discharge (Segal, Rogawski, & Barker, 1984). Such inhibition has been associated with a closed-state

dependent block (e.g., Armstrong & Loboda, 2001). This is also true for Kv1.5 (Bouchard & Fedida, 1995). Thus, closed-state inhibition of Kv1.5 channels in the present thesis could be partially responsible for the rescue of repetitive firing. Interestingly, several (tricyclic) antidepressants have been shown to inhibit Kv channels in general, among them nortriptyline, structurally very similar to protriptyline (H. Li et al., 2018; Shin et al., 2017), or to inhibit Kv1.5 channels specifically (H. M. Lee, Hahn, & Choi, 2016).

The detrimental effects of a higher concentration of protriptyline (Fig **4.1.5**) also evidence a Kv1.5 channel block by protriptyline. Substantial inhibition of Kv channels induces membrane depolarization (in arterial smooth muscle cells, Bae et al., 2006; Shimoda, Sylvester, & Sham, 1998). This could promote the occurrence of a depolarization block, causing action potential numbers and amplitudes to drop even further and compromising the ability to repolarize in all neurons (Fig **4.1.5**). In line with this, membrane-depolarizing agents have been involved in the inactivation of sodium channels and failure to initiate action potentials, for example, at the neuromuscular junction (Lingle & Steinbach, 1988).

This emphasizes the need for a fine-tuned inhibition within a range that reduces Kv channel currents just enough to increase the firing rate but does not depolarize the membrane to a level detrimental to the ability to fire.

5.1.4 Limitations

In this thesis, I have only investigated neurons in the PL of the mPFC. However, to strengthen the hypothesized association of protriptyline with impulsivity, it would be of use to also explore neurons in the IL, shown to be a bigger hub for impulsivity than the PL (Chudasama, 2011; Chudasama et al., 2003; Jupp et al., 2013; Robbins, 2002; Sokolowski & Salamone, 1994). However, only one test of the PsyCoP battery (Volkmann et al., 2020) *Neurod6* KO mice were subjected to involved the assessment of impulsivity, namely, of waiting – and, thus, rather IL-related impulsivity. These mice may show deficits in impulse control in other, rather PL-related, areas that were not assessed.

Furthermore, the present electrophysiological studies were not conducted on behaviorally-characterized cohorts of mice, but on naïve mice. Thus, electrophysiological phenotypes could not directly be correlated with behavioral impairment.

In general, only correlations between *Neurod6* KO, impulsivity, protriptyline, and sustained action potential firing have been assessed: Electrophysiological and behavioral (rescue) experiments were done separately. To solidify a link between both, it would be valuable, for example, to investigate neuronal activity in mPFC PL L5 neurons in protriptyline- and placebo-treated *Neurod6* KO mice *in vivo* during a behavioral test of impulsivity. It may also be valuable to focus on L5 neurons with specific

projection targets. For example, Li, Nguyen, Ma, and Dan (2020) showed that L5 neurons projecting to the STN have a specialized role in inhibiting habitual responses, whereas overactivation or insufficient inhibition of LH-projecting L5 neurons increases impulsive behavior. Given that the data reported in this thesis can be split into phenotypic and non-phenotypic neurons, it would be helpful to see if these phenotype- and projection-target-defined populations overlap. For example, STN-projecting neurons could be mostly phenotypic, and LH-projecting neurons non-phenotypic.

The effects of protriptyline on behavior and neuronal physiology in the present studies in *Neurod6* KO mice may include serotonin and norepinephrine reuptake and receptor inhibition. Due to reuptake inhibition, serotonin extracellular concentration is increased. However, serotonin 2A receptors are blocked, thus, transmission is inhibited. Reduced serotonin neurotransmission is important in the context of the hypothesis of upregulated serotonergic pathways in the prefrontal cortex in schizophrenia. This upregulation was suggested to contribute to cognitive impairment indirectly by downregulating dopamine activity. A decreased neurotransmission of serotonin, however, disinhibits the dopamine system, in the striatum as well as in the prefrontal cortex (Kapur & Remington, 1996). Stahl (2003) hypothesizes that blocking norepinephrine transporters leads to an increase in dopamine levels in the prefrontal cortex as well: As dopamine transporters are absent, extracellular dopamine can only be inactivated via norepinephrine transporters. If these are blocked, dopamine is free to diffuse extensively throughout the prefrontal cortex, leading to improvements in overall cognition. For example, norepinephrine reuptake inhibitors have been implicated in reducing hyperactive and impulsive symptoms in ADHD (Michelson et al., 2003; Michelson et al., 2002). However, it is unlikely that the rescue of repetitive firing in *Neurod6* KO neurons via protriptyline was due to effects on either serotonin or norepinephrine and, subsequently, dopamine neurotransmission. DPO-1 does not directly affect these transmitter systems. The almost identical rescue profiles of DPO-1 and protriptyline strongly indicate the same mode of action (Fig. **4.1.4**). Additionally, murine mPFC brain slices did not include brain areas homologous to VTA, locus coeruleus, or raphe nuclei, where dopamine, norepinephrine, and serotonin are produced in the human brain. A few neurotransmitters may have remained in the slice, however, a high influence on neuronal activity is unlikely.

Additionally, it should be noted that the data currently underlying KO- and rescue effect on action potential amplitudes only include neurons that fired at least 5 action potentials. I have not investigated these effects in severely affected neurons firing even less action potentials.

Finally, to exclude the possibility that the observed phenotypes are due to any other genetic variation in the *Neurod6* KO mouse line, it would be necessary to reintroduce the *Neurod6* gene into KO mice. However, this is very hard, if not impossible, to achieve.

5.1.5 Conclusions and outlook

In the first part of this thesis, I identified electrophysiological phenotypes in PL L5 neurons in the mPFC of *Neurod6* KO mice, accompanying their behavioral hyperactivity and increased behavioral impulsivity: Neurons were hyperexcitable, and use-dependent action potential generation was disturbed. The latter is likely related to the increased behavioral impulsivity: both sustained firing and impulsivity were selectively rescued by protriptyline and DPO-1, possibly via a Kv1.5 channel block.

Protriptyline has been approved for the treatment of depression, narcolepsy, ADHD, and headaches (Bansode et al., 2014). However, the data presented in this thesis suggest, for the first time, that protriptyline might block Kv1.5 channels in mPFC neurons in a mouse model of schizophrenia. Schizophrenia-related impulsive behavior in this mouse model might be related to an inability of a group of mPFC neurons to sustain a high firing rate of action potentials at physiological synaptic input currents. This may be due in part to an increased input resistance or to altered sodium and potassium channel dynamics of the involved neurons – or to a combination of both – and ultimately leads to network dysconnectivity. A Kv1.5 channel block, however, may increase the firing rate, and, thus, enhance communication between impulsivity-related brain areas.

In summary, protriptyline, or other antidepressants capable of blocking Kv channels, are promising candidates for further research regarding the treatment of executive dysfunction in schizophrenia. Furthermore, because the prevalence of comorbidity between schizophrenia and depression is high (Buckley, Miller, Lehrer, & Castle, 2009), adjunctive therapy with such antidepressants could be an added benefit. Additionally, it will be necessary to investigate the root causes of the increased input resistance and – if true – of the hypothesized alterations of sodium and potassium channel dynamics in *Neurod6* PL L5 neurons (Fig. **4.1.1.C**). These are likely to be at the core of the phenotypes described, and exploring potential treatment options will be invaluable. In addition, the reason for the hypothesized beneficial effect of a Kv1.5 channel block by protriptyline on sustained action potential firing needs to be further investigated. Currently, a comprehensive explanation is lacking.

5.2. Cre-conditional KO of *Taok2* affects cultured primary cortical neurons but not L5 neurons of the PL

In the second part of this thesis, I focused on morphological complexity and circuit integration of L5 neurons in acute slices of the PL of the mPFC in the *Taok2* x Emx1-Cre KO mouse and on morphological complexity of primary cortical neuronal cultures from these mice, answering the following questions (see section 1.3):

Research question 2.1

Is the morphological complexity and circuit integration of PL L5 neurons disturbed?

Research question 2.2

Is the morphological complexity of primary cortical neurons in culture disturbed?

In summary, no effect of cre-conditional *Taok2* KO on the morphological complexity or the circuit integration of PL L5 neurons was observed. However, cultured primary cortical neurons were morphologically underdeveloped.

5.2.1 Compensatory mechanisms counteracting Taok2 loss-of-function in the Taok2 x Emx1-Cre KO mouse

Surprisingly, and despite a large body of evidence (de Anda et al., 2012; Richter et al., 2019; Ultanir et al., 2014), I could not replicate underdeveloped dendritic morphology or synaptic dysconnectivity in L5 PL neurons of the mPFC (Fig. **4.2.1**). However, Ultanir et al. (2014), for example, report effects on spine development and maintenance based on TAOK2 and TAOK1 downregulation. Here, TAOK1 expression was not affected. Due to its involvement in similar molecular pathways and functions (Fang et al., 2020), TAOK1 upregulation *in vivo* might compensate for *Taok2* loss-of-function. Additionally, *Taok2* loss-of-function was shown by colleagues at the clinic to primarily affect MAPK and downstream signaling involving the ERK and p38 but not the JNK pathway. However, effects on dendrite formation, for example, have implicated the JNK1 pathway (de Anda et al., 2012).

It also needs to be considered that, contrary to previously reported studies, *Taok2* is not downregulated in cortical interneurons in the *Taok2*xEmx1-Cre KO mouse: Emx1 expression, and, thus, *Taok2* KO, is restricted to cortical pyramidal neurons (Chan et al., 2001). Importantly, GABAergic interneuron-pyramidal neuron communication involves the $GABA_B$ receptor, and this G protein-coupled receptor has been implied in MAPK pathway activation specifically involving ERK and JNK (Kanbara et al., 2018; Y. Wang et al., 2021) – like TAO kinases (colleagues at the clinic, unpublished, and Fang et al., 2020). The effect of *Taok2* downregulation on cortical interneurons has not been investigated in-depth. However, Willis, Pratt, and Morris (2021), for example, showed TAOK2-JNK

signaling to be involved in the maturation of cortical interneurons. The authors demonstrated adverse effects of an over-activation of this pathway and pharmacological TAOK and ERK inhibition on interneuronal gene expression, altering interneuronal development and possibly network activity. In the *Taok2*xEmx1-Cre KO mouse, interneurons may develop normally and partially counteract *Taok2* loss-of-function in pyramidal neurons via $GABA_B$ receptor signaling.

These compensatory mechanisms may be particularly important during *in vivo* brain development, as neurons in culture do not receive naturalistic inputs. However, naturalistic inputs are important for functional network formation and adaptive processes. This may explain the observed discrepancy between the findings in PL L5 neurons reported in this thesis (Fig. **4.2.1**) and the findings in primary cortical neurons in the literature as well as in this thesis (Fig. **4.2.2**).

5.2.2. Taok2 loss-of-function might affect PL L3 neurons instead of L5 neurons

Similar to the reduced morphological complexity of primary cortical neurons in mature cultures observed in this thesis (Fig. **4.2.2**), De Anda et al. (2012) reported adverse effects of TAOK2 downregulation on the morphology of developing cortical neurons in culture. Cortical cultures are prepared once cortical layer formation has already taken place, and they include neurons from various cortical areas and layers (Sahu et al., 2019). In this thesis, I have investigated the effects of TAOK2 downregulation specifically on PL L5 neurons of the mPFC. It may be that effects discovered in cortical neuronal cultures are mainly driven by L2/3 neurons. L2/3 pyramidal neurons are the most abundant cells of the neocortex (Zilles, 1990), thus, they are overrepresented in studies using cortical cultures as model system. Evidence supporting this hypothesis comes from findings in cortical neurons *ex vivo* or in acute slices (de Anda et al., 2012; Richter et al., 2019; Ultanir et al., 2014). All of these studies found effects of TAOK2 downregulation either on cortical neurons in general (de Anda et al., 2012) or on L2/3 neurons specifically, in the PL or in general (Richter et al., 2019; Ultanir et al., 2014). In line with this, Scharrenberg et al. (2022) found that TAOK2 was relevant for upper, but not for lower, cortical layer formation during development. However, it needs to be noted that de Anda et al (2012) did demonstrate a reduced basal dendritic complexity in L5 neurons specifically.

5.2.3 Limitations

Both primary cortical neurons and PL L5 neurons in this thesis were manually reconstructed, and spines were counted manually as well. This approach has two major disadvantages: It is time-consuming and error-prone due to subjectivity and potential inaccuracy. To minimize errors, one should compare results to those obtained using one of the available automated algorithms (for a review, see Donohue & Ascoli, 2011; Rodriguez et al., 2003; Zhao et al., 2011) or to those obtained by a second, independent person. Regarding the former, an open community bench-testing platform (BigNeuron) has been developed very recently to set open standards for accurate and fast automatic neuron reconstruction. It can generate consensus reconstructions across different algorithms outperforming single algorithms (Manubens-Gil et al., 2023). Thus, it might prove to be a valuable tool in the future.

Furthermore, the data set on PL L5 neurons is relatively small. However, due to the consistency of results across different, interrelated measures, it is most likely unambiguous.

Finally, it should be mentioned that colleagues at the clinic found that *Taok2* x Emx1-Cre KO mice showed only mild hyperactivity and anxiety phenotypes and no cognitive deficits. Thus, it is conceivable that they present very little change in neuronal morphology in any cortical layer or area.

5.2.4 Conclusions and outlook

In conclusion, the *Taok2* x Emx1-Cre KO mouse model may be more relevant for the study of cellular signaling pathways affected by a pyramidal-cell-specific KO of *Taok2* than as a model of cognitive impairment in schizophrenia. Nonetheless, these results highlight the importance of compensatory mechanisms counteracting *Taok2* KO *in vivo*, possibly ensuring a relatively high level of behavioral functioning in *Taok2* x Emx1-Cre KO mice. Whether these mechanisms rely more on the activity of other TAOKs like TAOK1, on cortical interneurons, or a combination of both, remains to be investigated. However, it must be emphasized that in all studies to date reporting aberrant morphology in cortical neurons *ex vivo*, behavioral deficits in the live mouse, or both (de Anda et al., 2012; Richter et al., 2019; Ultanir et al., 2014), *Taok2* was downregulated in interneurons as well as in pyramidal neurons and other cell types. Furthermore, some of those studies reported adverse effects of *Taok2* KO even in the presence of TAOK1 (de Anda et al., 2012; Richter et al., 2019). This opens up exciting new avenues of research into the interaction of different cell types and TAOKs in the maintenance of neuronal morphology, connectivity, and cognitive function in schizophrenia.

5.3 Summary

This thesis contributes to a better understanding of the cellular correlates of cognitive symptoms in schizophrenia, emphasizing the potential role of neuronal excitability and sustained action potential firing in PL L5 neurons of the mPFC in regulating impulsive behavior in a mouse model. The data presented in this thesis also suggest, for the first time, that the tricyclic antidepressant protriptyline may act via inhibition of voltage-gated potassium channels in rescuing the sustained firing capability of neurons potentially involved in executive function. Furthermore, this thesis raises the question of mechanisms compensating for *Taok2* loss of function in cortical pyramidal neurons in the live organism, preventing aberrant neuronal morphology and possibly aberrant connectivity involved in cognitive dysfunction.

6 Supplementary material

6.1 Supplementary material for section 4.1

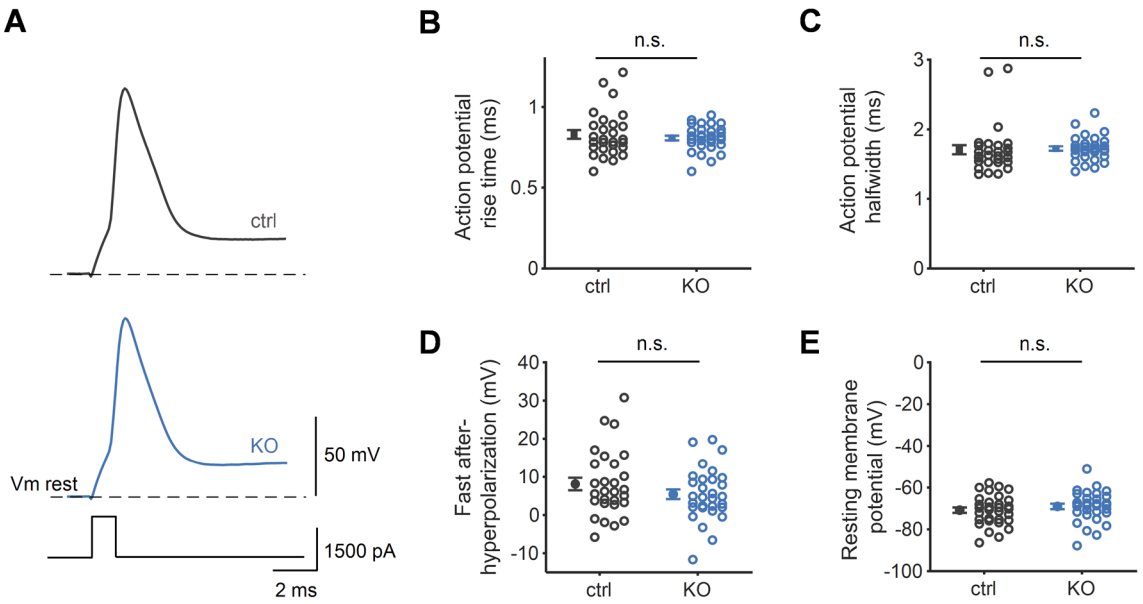

Supplementary figure 6.1.1 There is no influence of *Neurod6* KO on single action potential shape.

A. Example action potentials in response to a 1 ms long current injection of +1500 pA. Dashed line, Vm rest. **B.** There was no significant difference in action potential rise time between KO (n = 30) and ctrl (n = 28), P = .46. **C.** There was no significant difference in action potential half-width between KO (n = 30) and ctrl (n = 28), P = .10. **D.** There was no significant difference in fast afterhyperpolarization between KO (n = 30) and ctrl (n = 28), P = .20. **E.** There was no significant difference in resting membrane potential between KO (n = 31) and ctrl (n = 31), P = .34.

t-tests (two-tailed) and Wilcoxon rank-sum test (two-tailed). Filled circles and bars, means ± s.e.m., empty circles, individual neuron data.

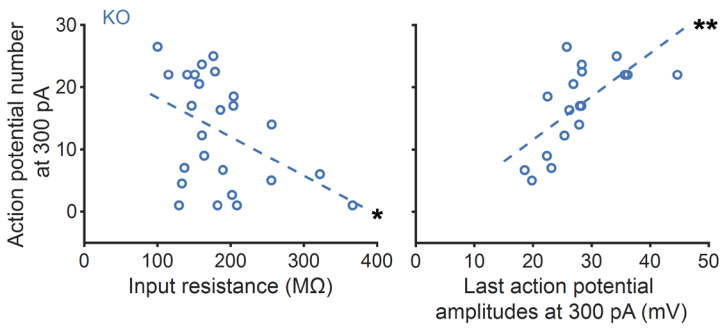

Supplementary figure 6.1.2 Input resistance and last action potential amplitudes predict action potential number.

Left, input resistance was negatively correlated with action potential number (n = 25), P = .029, R^2 = .19. Right, in KO neurons firing at least 5 action potentials at a current injection of +300pA, the amplitude of the last action potentials in the train was positively correlated with action potential number (n = 18), P = .003, R^2 = .44. Results are shown for a current injection of +300 pA because few KO neurons fired at least 5 action potentials at higher current injections. Thus, data on the amplitude of the last action potentials in a train at those current injections were too sparse.

Linear regressions. Empty circles, individual neuron data. Dashed line, linear fit.

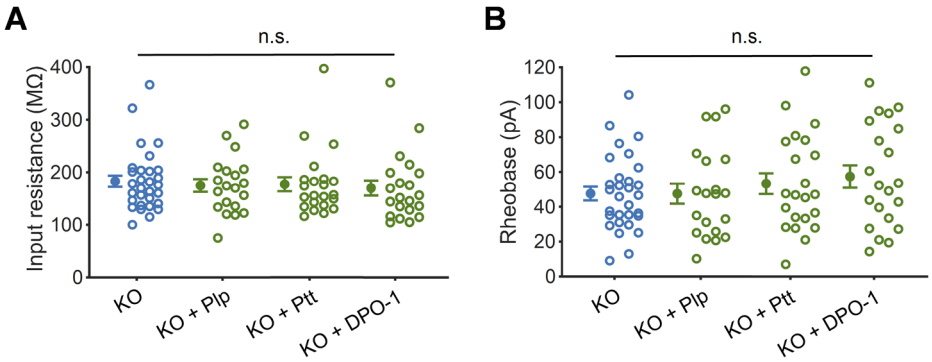

Supplementary figure 6.1.3 Neither paliperidone nor protriptyline or DPO-1 rescue neuronal hyperexcitability.

A. Input resistance was not significantly different between KO (n = 30), paliperidone-treated KO (n = 20), protriptyline-treated KO (n = 22), and DPO-1-treated KO neurons (n = 21), P = .77. **B.** Rheobase was not significantly different between KO (n = 30), paliperidone-treated KO (n = 20), protriptyline-treated KO (n = 22), and DPO-1-treated KO neurons (n = 21), P = .53.

Plp, paliperidone, *Ptt*, protriptyline. Kruskal-Wallis-test and one-way ANOVA. Filled circles and bars, means ± s.e.m, empty circles, individual neuron data.

6.2 Supplementary material for section 4.2

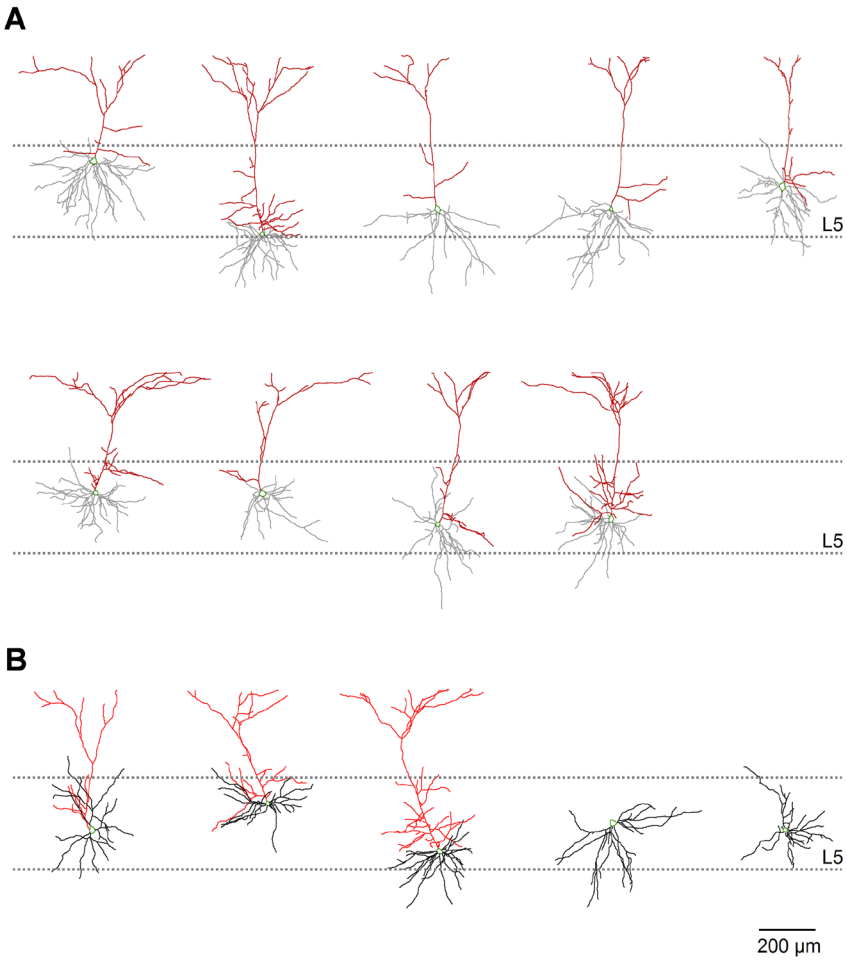

Supplementary figure 6.2.1 Reconstructed morphologies of *Taok2* KO and ctrl PL L5 neurons from acute slices. **A.** *Taok2* KO neurons. Grey, basal dendritic tree, dark red, apical dendritic tree. **B.** *Taok2* ctrl neurons. Black, basal dendritic tree, light red, apical dendritic tree. Soma outlines are indicated in green. Neurons in each row are oriented towards the pial surface at the top. L5 is encompassed by the grey dotted lines.

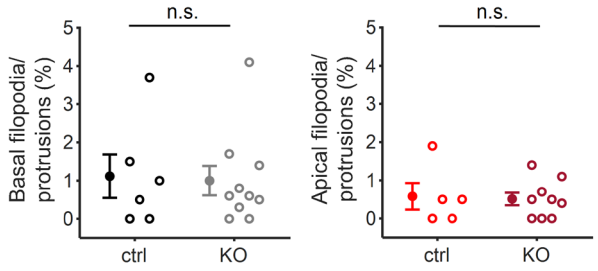

Supplementary figure 6.2.2 Cre-conditional *Taok2* KO does not affect the number of filopodia in PL L5 neurons in acute slices.

Left, the fraction of filopodia among the basal protrusions was not significantly different between ctrl (n = 6) and KO (n = 10), P = .98. Right, the fraction of filopodia among the apical protrusions was not significantly different between ctrl (n = 5) and KO (n = 9), P = 1.

Wilcoxon rank-sum tests (two-tailed). Filled circles and bars, means ± s.e.m., empty circles, individual neuron data.

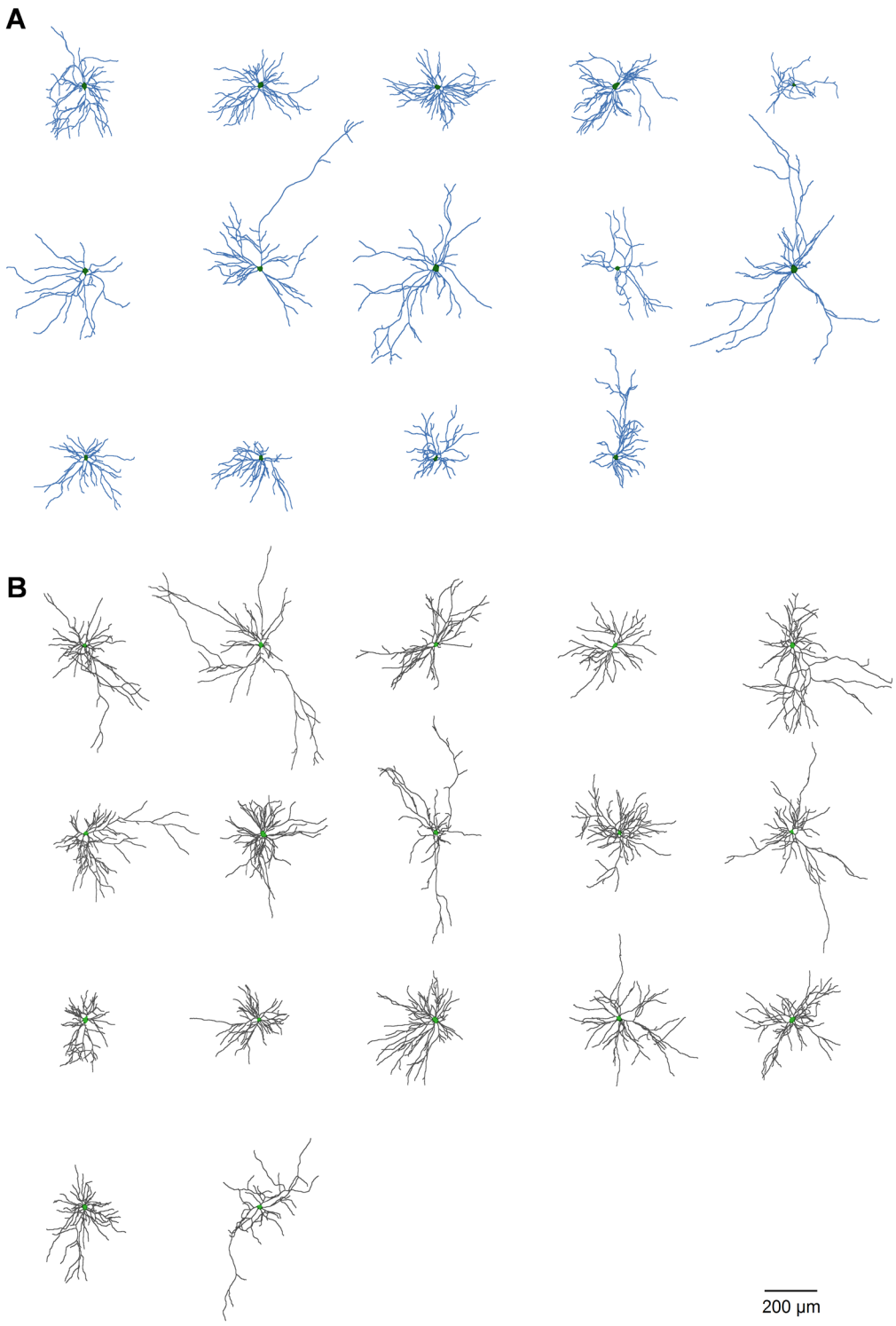

Supplementary figure 6.2.3 Reconstructed morphologies of cultured primary cortical *Taok2* KO and ctrl neurons.

A. *Taok2* KO neurons. Blue, dendritic tree, dark green, soma surface area. **B.** *Taok2* ctrl neurons. Dark grey, dendritic tree, light green, soma surface area.

Bibliography

Abi-Dargham, A., Mawlawi, O., Lombardo, I., Gil, R., Martinez, D., Huang, Y., . . . Laruelle, M. (2002). Prefrontal dopamine D1 receptors and working memory in schizophrenia. *Journal of Neuroscience, 22*(9), 3708-3719. doi:10.1523/JNEUROSCI.22-09-03708.2002

Agren, R., Nilsson, J., & Arhem, P. (2019). Closed and open state dependent block of potassium channels cause opposing effects on excitability - a computational approach. *Scientific Reports, 9*(1), 8175. doi:10.1038/s41598-019-44564-x

An, J. R., Kang, H., Li, H., Seo, M. S., Jung, H. S., Jung, W. K., . . . Park, W. S. (2020). Protriptyline, a tricyclic antidepressant, inhibits voltage-dependent K+ channels in rabbit coronary arterial smooth muscle cells. *Acta Biochimica et Biophysica Sinica, 52*(3), 320-327. doi:10.1093/abbs/gmz159

Andreasen, N. C., Paradiso, S., & O'Leary, D. S. (1998). "Cognitive dysmetria" as an integrative theory of schizophrenia: A dysfunction in cortical-subcortical-cerebellar circuitry? *Schizophrenia Bulletin, 24*(2), 203-218. doi:10.1093/oxfordjournals.schbul.a033321

Arion, D., Corradi, J. P., Tang, S., Datta, D., Boothe, F., He, A., . . . Lewis, D. A. (2015). Distinctive transcriptome alterations of prefrontal pyramidal neurons in schizophrenia and schizoaffective disorder. *Molecular Psychiatry, 20*(11), 1397-1405. doi:10.1038/mp.2014.171

Armstrong, C. M. (2006). Na channel inactivation from open and closed states. *PNAS, 103*(47), 17991-17996. doi:10.1073/pnas.0607603103

Armstrong, C. M., & Loboda, A. (2001). A model for 4-aminopyridine action on K channels: similarities to tetraethylammonium ion action. *Biophysical Journal, 81*(2), 895-904. doi:10.1016/S0006-3495(01)75749-9

Arsenault, D., Julien, C., Tremblay, C., & Calon, F. (2011). DHA improves cognition and prevents dysfunction of entorhinal cortex neurons in 3xTg-AD mice. *PLoS One, 6*(2), e17397. doi:10.1371/journal.pone.0017397

Badcock, J. C., Michie, P. T., Johnson, L., & Combrinck, J. (2002). Acts of control in schizophrenia: dissociating the components of inhibition. *Psychological Medicine, 32*(2), 287-297. doi:10.1017/s0033291701005128

Bae, Y. M., Kim, A., Kim, J., Park, S. W., Kim, T. K., Lee, Y. R., . . . Cho, S. I. (2006). Serotonin depolarizes the membrane potential in rat mesenteric artery myocytes by decreasing voltage-gated K+ currents. *Biochemical and Biophysical Research Communications, 347*(2), 468-476. doi:10.1016/j.bbrc.2006.06.116

Bansode, S. B., Jana, A. K., Batkulwar, K. B., Warkad, S. D., Joshi, R. S., Sengupta, N., & Kulkarni, M. J. (2014). Molecular investigations of protriptyline as a multi-target directed ligand in Alzheimer's disease. *PLoS One, 9*(8), e105196. doi:10.1371/journal.pone.0105196

Barnett, J. H., Jones, P. B., Robbins, T. W., & Muller, U. (2007). Effects of the catechol-O-methyltransferase Val158Met polymorphism on executive function: A meta-analysis of the Wisconsin Card Sort Test in schizophrenia and healthy controls. *Molecular Psychiatry, 12*(5), 502-509. doi:10.1038/sj.mp.4001973

Bianchi, D., Marasco, A., Limongiello, A., Marchetti, C., Marie, H., Tirozzi, B., & Migliore, M. (2012). On the mechanisms underlying the depolarization block in the spiking dynamics of CA1 pyramidal neurons. *Journal of Computational Neuroscience, 33*(2), 207-225. doi:10.1007/s10827-012-0383-y

Bissonette, G. B., Powell, E. M., & Roesch, M. R. (2013). Neural structures underlying set-shifting: roles of medial prefrontal cortex and anterior cingulate cortex. *Behavoural Brain Research, 250*, 91-101. doi:10.1016/j.bbr.2013.04.037

Blasi, G., Goldberg, T. E., Weickert, T., Das, S., Kohn, P., Zoltick, B., . . . Mattay, V. S. (2006). Brain regions underlying response inhibition and interference monitoring and suppression. *European Journal of Neuroscience, 23*(6), 1658-1664. doi:10.1111/j.1460-9568.2006.04680.x

Bonvicini, C., Faraone, S. V., & Scassellati, C. (2018). Common and specific genes and peripheral biomarkers in children and adults with attention-deficit/hyperactivity disorder. *The World Journal of Biological Psychiatry, 19*(2), 80-100. doi:10.1080/15622975.2017.1282175

Bormuth, I., Yan, K., Yonemasu, T., Gummert, M., Zhang, M., Wichert, S., . . . Schwab, M. H. (2013). Neuronal basic helix-loop-helix proteins Neurod2/6 regulate cortical commissure formation before midline interactions. *Journal of Neuroscience, 33*(2), 641-651. doi:10.1523/JNEUROSCI.0899-12.2013

Bouchard, R., & Fedida, D. (1995). Closed- and open-state binding of 4-aminopyridine to the cloned human potassium channel Kv1.5. *Journal of Pharmacology and Experimental Therapeutics, 275*(2), 864-876. Retrieved from https://www.ncbi.nlm.nih.gov/pubmed/7473178

Brozoski, T. J., Brown, R. M., Rosvold, H. E., & Goldman, P. S. (1979). Cognitive deficit caused by regional depletion of dopamine in prefrontal cortex of rhesus monkey. *Science, 205*(4409), 929-932. doi:10.1126/science.112679

Buckley, P. F., Miller, B. J., Lehrer, D. S., & Castle, D. J. (2009). Psychiatric comorbidities and schizophrenia. *Schizophrenia Bulletin, 35*(2), 383-402. doi:10.1093/schbul/sbn135

Chan, C. H., Godinho, L. N., Thomaidou, D., Tan, S. S., Gulisano, M., & Parnavelas, J. G. (2001). Emx1 is a marker for pyramidal neurons of the cerebral cortex. *Cerebral Cortex, 11*(12), 1191-1198. doi:10.1093/cercor/11.12.1191

Charlson, F. J., Ferrari, A. J., Santomauro, D. F., Diminic, S., Stockings, E., Scott, J. G., . . . Whiteford, H. A. (2018). Global Epidemiology and Burden of Schizophrenia: Findings From the Global Burden of Disease Study 2016. *Schizophrenia Bulletin, 44*(6), 1195-1203. doi:10.1093/schbul/sby058

Chudasama, Y. (2011). Animal models of prefrontal-executive function. *Behavioral Neuroscience, 125*(3), 327-343. doi:10.1037/a0023766

Chudasama, Y., Passetti, F., Rhodes, S. E., Lopian, D., Desai, A., & Robbins, T. W. (2003). Dissociable aspects of performance on the 5-choice serial reaction time task following lesions of the dorsal anterior cingulate, infralimbic and orbitofrontal cortex in the rat: Differential effects on selectivity, impulsivity and compulsivity. *Behavioural Brain Research, 146*(1-2), 105-119. doi:10.1016/j.bbr.2003.09.020

Cirillo, M. A., & Seidman, L. J. (2003). Verbal declarative memory dysfunction in schizophrenia: From clinical assessment to genetics and brain mechanisms. *Neuropsychology Review, 13*(2), 43-77. doi:10.1023/a:1023870821631

Clark, L., Cools, R., & Robbins, T. W. (2004). The neuropsychology of ventral prefrontal cortex: Decision-making and reversal learning. *Brain and Cognition, 55*(1), 41-53. doi:10.1016/S0278-2626(03)00284-7

Cramer, C. L., Stagnitto, M. L., Knowles, M. A., & Palmer, G. C. (1994). Kainic acid and 4-aminopyridine seizure models in mice: Evaluation of efficacy of anti-epileptic agents and calcium antagonists. *Life Sciences, 54*(16), PL271-275. doi:10.1016/0024-3205(94)00845-0

Cuntz, H., Forstner, F., Borst, A., & Hausser, M. (2011). The TREES toolbox--probing the basis of axonal and dendritic branching. *Neuroinformatics, 9*(1), 91-96. doi:10.1007/s12021-010-9093-7

Dalley, J. W., Cardinal, R. N., & Robbins, T. W. (2004). Prefrontal executive and cognitive functions in rodents: neural and neurochemical substrates. *Neuroscience & Biobehavioral Reviews, 28*(7), 771-784. doi:10.1016/j.neubiorev.2004.09.006

de Anda, F. C., Rosario, A. L., Durak, O., Tran, T., Graff, J., Meletis, K., . . . Tsai, L. H. (2012). Autism spectrum disorder susceptibility gene TAOK2 affects basal dendrite formation in the neocortex. *Nature Neuroscience, 15*(7), 1022-1031. doi:10.1038/nn.3141

DeNardo, L. A., Berns, D. S., DeLoach, K., & Luo, L. (2015). Connectivity of mouse somatosensory and prefrontal cortex examined with trans-synaptic tracing. *Nature Neuroscience, 18*(11), 1687-1697. doi:10.1038/nn.4131

Donohue, D. E., & Ascoli, G. A. (2011). Automated reconstruction of neuronal morphology: an overview. *Brain Research Reviews, 67*(1-2), 94-102. doi:10.1016/j.brainresrev.2010.11.003

Du, Y. M., Zhang, X. X., Tu, D. N., Zhao, N., Liu, Y. J., Xiao, H., . . . Liao, Y. H. (2010). Molecular determinants of Kv1.5 channel block by diphenyl phosphine oxide-1. *Journal of Molecular and Cellular Cardiology, 48*(6), 1111-1120. doi:10.1016/j.yjmcc.2010.02.010

Enticott, P. G., Ogloff, J. R., & Bradshaw, J. L. (2008). Response inhibition and impulsivity in schizophrenia. *Psychiatry Research, 157*(1-3), 251-254. doi:10.1016/j.psychres.2007.04.007

Euston, D. R., Gruber, A. J., & McNaughton, B. L. (2012). The role of medial prefrontal cortex in memory and decision making. *Neuron, 76*(6), 1057-1070. doi:10.1016/j.neuron.2012.12.002

Fang, C. Y., Lai, T. C., Hsiao, M., & Chang, Y. C. (2020). The Diverse Roles of TAO Kinases in Health and Diseases. *International Journal of Molecular Sciences, 21*(20). doi:10.3390/ijms21207463

Farkas, T., Wolf, A. P., Jaeger, J., Brodie, J. D., Christman, D. R., & Fowler, J. S. (1984). Regional brain glucose metabolism in chronic schizophrenia. A positron emission transaxial tomographic study. *Archives of General Psychiatry, 41*(3), 293-300. doi:10.1001/archpsyc.1984.01790140083010

Feja, M., & Koch, M. (2015). Frontostriatal systems comprising connections between ventral medial prefrontal cortex and nucleus accumbens subregions differentially regulate motor impulse control in rats. *Psychopharmacology, 232*(7), 1291-1302. doi:10.1007/s00213-014-3763-3

Friston, K. J. (1998). The disconnection hypothesis. *Schizophrenia Research, 30*(2), 115-125. doi:10.1016/s0920-9964(97)00140-0

Gerstner, W., Kistler, W. M., Naud, R., & Paninski, L. (2014). *Neuronal Dynamics: from single neurons to networks and models of cognition and beyond.* Cambridge, UK: Cambridge University Press.

Gut-Fayand, A., Dervaux, A., Olie, J. P., Loo, H., Poirier, M. F., & Krebs, M. O. (2001). Substance abuse and suicidality in schizophrenia: A common risk factor linked to impulsivity. *Psychiatry Research, 102*(1), 65-72. doi:10.1016/s0165-1781(01)00250-5

Heerey, E. A., Robinson, B. M., McMahon, R. P., & Gold, J. M. (2007). Delay discounting in schizophrenia. *Cognitive Neuropsychiatry, 12*(3), 213-221. doi:10.1080/13546800601005900

Heidbreder, C. A., & Groenewegen, H. J. (2003). The medial prefrontal cortex in the rat: Evidence for a dorso-ventral distinction based upon functional and anatomical characteristics. *Neuroscience & Biobehavioral Reviews, 27*(6), 555-579. doi:10.1016/j.neubiorev.2003.09.003

Henley, K. (2021). *Foundations of neuroscience: open edition*. Retrieved from https://openbooks.lib.msu.edu/neuroscience/

Ingvar, D. H., & Franzen, G. (1974). Distribution of cerebral activity in chronic schizophrenia. *Lancet, 2*(7895), 1484-1486. doi:10.1016/s0140-6736(74)90221-9

Jaaskelainen, E., Juola, P., Hirvonen, N., McGrath, J. J., Saha, S., Isohanni, M., . . . Miettunen, J. (2013). A systematic review and meta-analysis of recovery in schizophrenia. *Schizophrenia Bulletin, 39*(6), 1296-1306. doi:10.1093/schbul/sbs130

Callicott, J. H., Mattay, V.S., Verchinski, B. A., Marenco, S., Egan, M. F., & Weinberger, D. R. (2003). Complexity of Prefrontal Cortical Dysfunction in Schizophrenia: More Than Up or Down. *American Journal of Psychiatry, 160*(12), 2209–2215). doi:10.1176/appi.ajp.160.12.2209

Jung, H. Y., Jung, S., Bang, M., Choi, T. K., Park, C. I., & Lee, S. H. (2022). White matter correlates of impulsivity in frontal lobe and their associations with treatment response in first-episode schizophrenia. *Neuroscience Letters, 767*, 136309. doi:10.1016/j.neulet.2021.136309

Jupp, B., Caprioli, D., Saigal, N., Reverte, I., Shrestha, S., Cumming, P., . . . Dalley, J. W. (2013). Dopaminergic and GABA-ergic markers of impulsivity in rats: Evidence for anatomical localisation in ventral striatum and prefrontal cortex. *European Journal of Neuroscience, 37*(9), 1519-1528. doi:10.1111/ejn.12146

Kaladjian, A., Jeanningros, R., Azorin, J. M., Anton, J. L., & Mazzola-Pomietto, P. (2011). Impulsivity and neural correlates of response inhibition in schizophrenia. *Psychological Medicine, 41*(2), 291-299. doi:10.1017/S0033291710000796

Kanbara, K., Otsuki, Y., Watanabe, M., Yokoe, S., Mori, Y., Asahi, M., & Neo, M. (2018). GABA(B) receptor regulates proliferation in the high-grade chondrosarcoma cell line OUMS-27 via apoptotic pathways. *BMC Cancer, 18*(1), 263. doi:10.1186/s12885-018-4149-4

Kantrowitz, J. T., & Javitt, D. C. (2010). N-methyl-d-aspartate (NMDA) receptor dysfunction or dysregulation: The final common pathway on the road to schizophrenia? *Brain Research Bulletin, 83*(3-4), 108-121. doi:10.1016/j.brainresbull.2010.04.006

Kapur, S., & Remington, G. (1996). Serotonin-dopamine interaction and its relevance to schizophrenia. *American Journal of Psychiatry, 153*(4), 466-476. doi:10.1176/ajp.153.4.466

Keefe, R. S., Bilder, R. M., Davis, S. M., Harvey, P. D., Palmer, B. W., Gold, J. M., . . . Neurocognitive Working, G. (2007). Neurocognitive effects of antipsychotic medications in patients with chronic schizophrenia in the CATIE Trial. *Archives of General Psychiatry, 64*(6), 633-647. doi:10.1001/archpsyc.64.6.633

Keefe, R. S., Eesley, C. E., & Poe, M. P. (2005). Defining a cognitive function decrement in schizophrenia. *Biological Psychiatry, 57*(6), 688-691. doi:10.1016/j.biopsych.2005.01.003

Kepa, A., Martinez Medina, L., Erk, S., Srivastava, D. P., Fernandes, A., Toro, R., . . . Desrivieres, S. (2017). Associations of the intellectual disability gene MYT1L with helix-loop-helix gene expression, hippocampus volume and hippocampus activation during memory retrieval. *Neuropsychopharmacology, 42*(13), 2516-2526. doi:10.1038/npp.2017.91

Kocsis, J. D., Eng, D. L., Gordon, T. R., & Waxman, S. G. (1987). Functional differences between 4-aminopyridine and tetraethylammonium-sensitive potassium channels in myelinated axons. *Neuroscience Letters, 75*(2), 193-198. doi:10.1016/0304-3940(87)90296-5

Kolb, B., & Whishaw, I. Q. (1983). Performance of schizophrenic patients on tests sensitive to left or right frontal, temporal, or parietal function in neurological patients. *The Journal of Nervous and Mental Disease, 171*(7), 435-443. doi:10.1097/00005053-198307000-00008

Leclerc, M. P., Regenbogen, C., Hamilton, R. H., & Habel, U. (2018). Some neuroanatomical insights to impulsive aggression in schizophrenia. *Schizophrenia Research, 201*, 27-34. doi:10.1016/j.schres.2018.06.016

Lee, F. H., Fadel, M. P., Preston-Maher, K., Cordes, S. P., Clapcote, S. J., Price, D. J., . . . Wong, A. H. (2011). Disc1 point mutations in mice affect development of the cerebral cortex. *Journal of Neuroscience, 31*(9), 3197-3206. doi:10.1523/JNEUROSCI.4219-10.2011

Lee, H. M., Hahn, S. J., & Choi, B. H. (2016). Blockade of Kv1.5 channels by the antidepressant drug sertraline. *The Korean Journal of Physiology & Pharmacology, 20*(2). doi:10.4196/kjpp.2016.20.2.193

Leysen, J. E., Niemegeers, C. J., Van Nueten, J. M., & Laduron, P. M. (1982). [3H]Ketanserin (R 41 468), a selective 3H-ligand for serotonin2 receptor binding sites. Binding properties, brain distribution, and functional role. *Molecular Pharmacology, 21*(2), 301-314. Retrieved from https://www.ncbi.nlm.nih.gov/pubmed/7099138

Li, B., Nguyen, T. P., Ma, C., & Dan, Y. (2020). Inhibition of impulsive action by projection-defined prefrontal pyramidal neurons. *PNAS, 117*(29), 17278-17287. doi:10.1073/pnas.2000523117

Li, H., Shin, S. E., An, J. R., Seo, M. S., Ha, K. S., Han, E. T., . . . Park, W. S. (2018). Blockade of voltage-dependent K(+) current in rabbit coronary arterial smooth muscle cells by the tricyclic antidepressant clomipramine. *Journal of Pharmacolical Sciences, 137*(1), 61-66. doi:10.1016/j.jphs.2018.04.005

Lieberman, J. A., Koreen, A. R., Chakos, M., Sheitman, B., Woerner, M., Alvir, J. M., & Bilder, R. (1996). Factors influencing treatment response and outcome of first-episode schizophrenia: implications for understanding the pathophysiology of schizophrenia. *Journal of Clinical Psychiatry, 57 Suppl 9*, 5-9. Retrieved from https://www.ncbi.nlm.nih.gov/pubmed/8823344

Lingle, C. J., & Steinbach, J. H. (1988). Neuromuscular blocking agents. *International Anesthesiology Clinics, 26*(4), 288-301. doi:10.1097/00004311-198802640-00007

Lipszyc, J., & Schachar, R. (2010). Inhibitory control and psychopathology: A meta-analysis of studies using the stop signal task. *Journal of the International Neuropsychological Society, 16*(6), 1064-1076. doi:10.1017/S1355617710000895

Manubens-Gil, L., Zhou, Z., Chen, H., Ramanathan, A., Liu, X., Liu, Y., . . . Peng, H. (2023). BigNeuron: A resource to benchmark and predict performance of algorithms for automated tracing of neurons in light microscopy datasets. *Nature Methods, 20*(6), 824-835. doi:10.1038/s41592-023-01848-5

McCarthy, S. E., Makarov, V., Kirov, G., Addington, A. M., McClellan, J., Yoon, S., . . . Sebat, J. (2009). Microduplications of 16p11.2 are associated with schizophrenia. *Nature Genetics, 41*(11), 1223-1227. doi:10.1038/ng.474

Michelson, D., Adler, L., Spencer, T., Reimherr, F. W., West, S. A., Allen, A. J., . . . Milton, D. (2003). Atomoxetine in adults with ADHD: Two randomized, placebo-controlled studies. *Biological Psychiatry, 53*(2), 112-120. doi:10.1016/s0006-3223(02)01671-2

Michelson, D., Allen, A. J., Busner, J., Casat, C., Dunn, D., Kratochvil, C., . . . Harder, D. (2002). Once-daily atomoxetine treatment for children and adolescents with attention deficit hyperactivity disorder: A randomized, placebo-controlled study. *American Journal of Psychiatry, 159*(11), 1896-1901. doi:10.1176/appi.ajp.159.11.1896

Minzenberg, M. J., Laird, A. R., Thelen, S., Carter, C. S., & Glahn, D. C. (2009). Meta-analysis of 41 functional neuroimaging studies of executive function in schizophrenia. *Archives of General Psychiatry, 66*(8), 811-822. doi:10.1001/archgenpsychiatry.2009.91

Nolan, K. A., D'Angelo, D., & Hoptman, M. J. (2011). Self-report and laboratory measures of impulsivity in patients with schizophrenia or schizoaffective disorder and healthy controls. *Psychiatry Research, 187*(1-2), 301-303. doi:10.1016/j.psychres.2010.10.032

Ouzir, M. (2013). Impulsivity in schizophrenia: a comprehensive update. *Aggress Violent Behav*, *18*(2), 247-254.

Paxinos, G. & Franklin, K. B. J. (2001). *The mouse brain in stereotaxic coordinates: hard cover edition*. Retrieved from http://labs.gaidi.ca/mouse-brain-atlas/

Pettersson-Yeo, W., Allen, P., Benetti, S., McGuire, P., & Mechelli, A. (2011). Dysconnectivity in schizophrenia: Where are we now? *Neuroscience & Biobehavioral Reviews, 35*(5), 1110-1124. doi:10.1016/j.neubiorev.2010.11.004

Ragland, J. D., Yoon, J., Minzenberg, M. J., & Carter, C. S. (2007). Neuroimaging of cognitive disability in schizophrenia: search for a pathophysiological mechanism. *International Review of Psychiatry, 19*(4), 417-427. doi:10.1080/09540260701486365

Ren, D. (2011). Sodium leak channels in neuronal excitability and rhythmic behaviors. *Neuron, 72*(6), 899-911. doi:10.1016/j.neuron.2011.12.007

Rho, J. M., Szot, P., Tempel, B. L., & Schwartzkroin, P. A. (1999). Developmental seizure susceptibility of kv1.1 potassium channel knockout mice. *Developmental Neuroscience, 21*(3-5), 320-327. doi:10.1159/000017381

Richelson, E., & Nelson, A. (1984). Antagonism by antidepressants of neurotransmitter receptors of normal human brain in vitro. *Journal of Pharmacology and Experimental Therapeutics, 230*(1), 94-102. Retrieved from https://www.ncbi.nlm.nih.gov/pubmed/6086881

Richter, M., Murtaza, N., Scharrenberg, R., White, S. H., Johanns, O., Walker, S., . . . Calderon de Anda, F. (2019). Altered TAOK2 activity causes autism-related neurodevelopmental and cognitive abnormalities through RhoA signaling. *Molecular Psychiatry, 24*(9), 1329-1350. doi:10.1038/s41380-018-0025-5

Robbins, T. W. (2000). From arousal to cognition: The integrative position of the prefrontal cortex. *Prog Brain Res, 126*, 469-483. doi:10.1016/S0079-6123(00)26030-5

Robbins, T. W. (2002). The 5-choice serial reaction time task: Behavioural pharmacology and functional neurochemistry. *Psychopharmacology, 163*(3-4), 362-380. doi:10.1007/s00213-002-1154-7

Rodriguez, A., Ehlenberger, D., Kelliher, K., Einstein, M., Henderson, S. C., Morrison, J. H., . . . Wearne, S. L. (2003). Automated reconstruction of three-dimensional neuronal morphology from laser scanning microscopy images. *Methods, 30*(1), 94-105. doi:10.1016/s1046-2023(03)00011-2

Sahu, M. P., Nikkila, O., Lagas, S., Kolehmainen, S., & Castren, E. (2019). Culturing primary neurons from rat hippocampus and cortex. *Neuronal Signalingl, 3*(2), NS20180207. doi:10.1042/NS20180207

Sakurai, T., Gamo, N. J., Hikida, T., Kim, S. H., Murai, T., Tomoda, T., & Sawa, A. (2015). Converging models of schizophrenia--Network alterations of prefrontal cortex underlying cognitive impairments. *Progress in Neurobiology, 134*, 178-201. doi:10.1016/j.pneurobio.2015.09.010

Scharrenberg, R., Richter, M., Johanns, O., Meka, D. P., Rucker, T., Murtaza, N., . . . de Anda, F. C. (2022). TAOK2 rescues autism-linked developmental deficits in a 16p11.2 microdeletion mouse model. *Molecular Psychiatry, 27*(11), 4707-4721. doi:10.1038/s41380-022-01785-3

Schwab, M. H., Druffel-Augustin, S., Gass, P., Jung, M., Klugmann, M., Bartholomae, A., . . . Nave, K. A. (1998). Neuronal basic helix-loop-helix proteins (NEX, neuroD, NDRF): spatiotemporal expression and targeted disruption of the NEX gene in transgenic mice. *Journal of Neuroscience, 18*(4), 1408-1418. doi:10.1523/JNEUROSCI.18-04-01408.1998

Segal, M., Rogawski, M. A., & Barker, J. L. (1984). A transient potassium conductance regulates the excitability of cultured hippocampal and spinal neurons. *Journal of Neuroscience, 4*(2), 604-609. doi:10.1523/JNEUROSCI.04-02-00604.1984

Shimoda, L. A., Sylvester, J. T., & Sham, J. S. (1998). Inhibition of voltage-gated K+ current in rat intrapulmonary arterial myocytes by endothelin-1. *American Journal of Physiology, 274*(5), L842-853. doi:10.1152/ajplung.1998.274.5.L842

Shin, S. E., Li, H., Kim, H. S., Kim, H. W., Seo, M. S., Ha, K. S., . . . Park, W. S. (2017). Nortriptyline, a tricyclic antidepressant, inhibits voltage-dependent K(+) channels in coronary arterial smooth muscle cells. *The Korean Journal of Physiology & Pharmacology, 21*(2), 225-232. doi:10.4196/kjpp.2017.21.2.225

Simpson, E. H., Kellendonk, C., & Kandel, E. (2010). A possible role for the striatum in the pathogenesis of the cognitive symptoms of schizophrenia. *Neuron, 65*(5), 585-596. doi:10.1016/j.neuron.2010.02.014

Singh, S. P., & Singh, V. (2011). Meta-analysis of the efficacy of adjunctive NMDA receptor modulators in chronic schizophrenia. *CNS Drugs, 25*(10), 859-885. doi:10.2165/11586650-000000000-00000

Sokolowski, J. D., & Salamone, J. D. (1994). Effects of dopamine depletions in the medial prefrontal cortex on DRL performance and motor activity in the rat. *Brain Research, 642*(1-2), 20-28. doi:10.1016/0006-8993(94)90901-6

Stahl, S. M. (2003). Neurotransmission of cognition, part 3. Mechanism of action of selective NRIs: Both dopamine and norepinephrine increase in prefrontal cortex. *Journal of Clinical Psychiatry, 64*(3), 230-231. Retrieved from https://www.ncbi.nlm.nih.gov/pubmed/12716261

Tatsumi, M., Groshan, K., Blakely, R. D., & Richelson, E. (1997). Pharmacological profile of antidepressants and related compounds at human monoamine transporters. *European Journal of Pharmacology, 340*(2-3), 249-258. doi:10.1016/s0014-2999(97)01393-9

Torres-Torrelo, J., Torres, B., & Carrascal, L. (2014). Modulation of the input-output function by GABAA receptor-mediated currents in rat oculomotor nucleus motoneurons. *Journal of Physiology, 592*(22), 5047-5064. doi:10.1113/jphysiol.2014.276576

Tran, V. T., Chang, R. S., & Snyder, S. H. (1978). Histamine H1 receptors identified in mammalian brain membranes with [3H]mepyramine. *PNAS, 75*(12), 6290-6294. doi:10.1073/pnas.75.12.6290

Turner, K. M., & Parkes, S. L. (2020). Prefrontal regulation of behavioural control: Evidence from learning theory and translational approaches in rodents. *Neuroscience & Biobehavioral Reviews, 118*, 27-41. doi:10.1016/j.neubiorev.2020.07.010

Ultanir, S. K., Yadav, S., Hertz, N. T., Oses-Prieto, J. A., Claxton, S., Burlingame, A. L., . . . Jan, Y. N. (2014). MST3 kinase phosphorylates TAO1/2 to enable Myosin Va function in promoting spine synapse development. *Neuron, 84*(5), 968-982. doi:10.1016/j.neuron.2014.10.025

Vertes, R. P. (2006). Interactions among the medial prefrontal cortex, hippocampus and midline thalamus in emotional and cognitive processing in the rat. *Neuroscience, 142*(1), 1-20. doi:10.1016/j.neuroscience.2006.06.027

Vijayraghavan, S., Wang, M., Birnbaum, S. G., Williams, G. V., & Arnsten, A. F. (2007). Inverted-U dopamine D1 receptor actions on prefrontal neurons engaged in working memory. *Nature Neuroscience, 10*(3), 376-384. doi:10.1038/nn1846

Volkmann, P., Stephan, M., Krackow, S., Jensen, N., & Rossner, M. J. (2020). PsyCoP - A platform for systematic semi-automated behavioral and cognitive profiling reveals gene and environment dependent impairments of Tcf4 transgenic mice subjected to social defeat. *Frontiers in Behavioral Neuroscience, 14*, 618180. doi:10.3389/fnbeh.2020.618180

Voskuyl, R. A., & Albus, H. (1985). Spontaneous epileptiform discharges in hippocampal slices induced by 4-aminopyridine. *Brain Research, 342*(1), 54-66. doi:10.1016/0006-8993(85)91352-6

Wallace, T. L., Ballard, T. M., Pouzet, B., Riedel, W. J., & Wettstein, J. G. (2011). Drug targets for cognitive enhancement in neuropsychiatric disorders. *Pharmacology Biochemistry and Behavior, 99*(2), 130-145. doi:10.1016/j.pbb.2011.03.022

Wang, L., Liang, P. J., Zhang, P. M., & Qiu, Y. H. (2014). Ionic mechanisms underlying tonic and phasic firing behaviors in retinal ganglion cells: A model study. *Channels, 8*(4), 298-307. doi:10.4161/chan.28012

Wang, Y., Gai, S., Zhang, W., Huang, X., Ma, S., Huo, Y., . . . Liu, J. (2021). The GABA(B) receptor mediates neuroprotection by coupling to G(13). *Science Signaling, 14*(705), eaaz4112. doi:10.1126/scisignal.aaz4112

Warchal, S. J., Dawson, J. C., Shepherd, E., Munro, A. F., Hughes, R. E., Makda, A., & Carragher, N. O. (2020). High content phenotypic screening identifies serotonin receptor modulators with selective activity upon breast cancer cell cycle and cytokine signaling pathways. *Bioorganic & Medicinal Chemistry, 28*(1), 115209. doi:10.1016/j.bmc.2019.115209

Weinberger, D. R., Berman, K. F., & Illowsky, B. P. (1988). Physiological dysfunction of dorsolateral prefrontal cortex in schizophrenia. III. A new cohort and evidence for a monoaminergic mechanism. *Archives of General Psychiatry, 45*(7), 609-615. doi:10.1001/archpsyc.1988.01800310013001

Willis, A., Pratt, J. A., & Morris, B. J. (2021). BDNF and JNK signaling modulate cortical interneuron and perineuronal net development: Implications for schizophrenia-linked 16p11.2 duplication syndrome. *Schizophrenia Bulletin, 47*(3), 812-826. doi:10.1093/schbul/sbaa139

Yasuda, S., Tanaka, H., Sugiura, H., Okamura, K., Sakaguchi, T., Tran, U., . . . Yamagata, K. (2007). Activity-induced protocadherin arcadlin regulates dendritic spine number by triggering N-cadherin endocytosis via TAO2beta and p38 MAP kinases. *Neuron, 56*(3), 456-471. doi:10.1016/j.neuron.2007.08.020

Zhao, T., Xie, J., Amat, F., Clack, N., Ahammad, P., Peng, H., . . . Myers, E. (2011). Automated reconstruction of neuronal morphology based on local geometrical and global structural models. *Neuroinformatics, 9*(2-3), 247-261. doi:10.1007/s12021-011-9120-3

Zhou, Y., Fan, L., Qiu, C., & Jiang, T. (2015). Prefrontal cortex and the dysconnectivity hypothesis of schizophrenia. *Neuroscience Bulletin, 31*(2), 207-219. doi:10.1007/s12264-014-1502-8

Zilles, K. (1990). Anatomy of the neocortex: cytoarchitecture and myeloarchitecture. In B. Kolb & R. C. Tees (Eds.), *The cerebral cortex of the rat* (pp. 77-113). Cambridge, MA: MIT.

Declaration of author contributions

Volker Scheuss and I designed all experiments. I carried out all experiments – preparation and data acquisition – and analyses.

Malgorzata Frydrych contributed to the preparation of experiments in *Neurod6* KO mice, subsequent electrophysiological recordings in *Neurod6* KO neurons in the presence of paliperidone, protriptyline, and DPO-1, and to their analysis under my guidance and close supervision.

Yun Wai Foo and Wenbo Ma helped reconstruct neuronal morphologies (5/31, Supplementary fig. **6.2.3**) under my guidance. I corrected and improved their respective reconstructions.

Wenbo Ma and Beate Kauschat prepared and maintained primary neuronal cultures of *Taok2* KO mice. Wenbo Ma performed virus infections of primary neurons.

Mouse lines were maintained and managed by Wilma Vogel, Jessica Bly, Pia Pickelmann, Philipp Schuler, and myself.

MATLAB analysis scripts were custom-written by Volker Scheuss and myself.

Acknowledgments

First and foremost, I would like to thank Volker Scheuss, my supervisor and Doktorvater, for the opportunity to work in your laboratory – special thanks to you for steering my inexperienced mind in the right direction! I enjoyed perfecting manuscripts and figures with you, and I enjoyed learning electrophysiology from you from scratch. You witnessed the first cells I patched (with many more to come), and you even introduced me to glass-making. We survived a lab move together during the peak of the Corona pandemic, and I witnessed the formation of what is now the Working Group of Synapse and Neural Circuit Physiology at the LMU Clinic for Psychiatry and Psychotherapy. I am delighted that we have grown so much as a lab.

I would also like to thank Therese Riedemann, who was always available for electrophysiological discussions, demonstrations, and help, and Volker Staiger, who taught me how to prepare organotypic cultures so well that it worked for me from the beginning. Acknowledgment must also be given to Vivek Sahoo, who was always there to help with cell culture-related questions. A special thanks goes to Susanne Koch and Oliver Bludau, I loved the many weekends spent working with you, and your advice helped a lot.

Many thanks go to my students Gosia and Yun Wai. It was a pleasure and lots of fun to work with you! Not only was I able to pass on my knowledge to you, but I also learned from you (who knew that you could pull your own microloaders!). Gosia, your hands-on approach was a breath of fresh air that I enjoyed a lot.

Now to my lab members, Elisanna, Amalya, and Felix: I loved those many late evenings and nights when we were all working (laughing and singing) together. Your company always elevated the mood and motivation 3-fold, and Amalya, you provided a great deal of good ideas! Big thanks also go to my friends, especially to Zeynep, who witnessed my PhD Journey and the many highs and lows from beginning to end. Thank you for the advice, and the many coffees and beers! You believed in me even during the toughest of times.

Finally, I am grateful for my family's unwavering support and understanding, especially (but not only!) during the end phase of my PhD, even supplying me with food and clothes when I was too busy to meet, celebrate, cook, or do laundry.

The success of this PhD, and many realizations about science and myself, is owed to all of you. I am very happy that all of you were part of this journey.